Master's thesis

NTNU
Norwegian University of Science and Technology
Faculty of Information Technology and Electrical Engineering
Department of Electronic Systems

Magnus Iben Holt

Non-Destructive Testing of Concrete

Comparing direct sound and coda measurement methods to analyze nonlinearities in ultrasonic sound speed response to distinguish concrete samples of different degradation grades

Master's thesis in Elektronisk Systemdesign og Innovasjon
Supervisor: Guillaume Dutilleux
Co-supervisor: Tonni Franke Johansen
August 2021

NTNU
Norwegian University of Science and Technology

Magnus Iben Holt

Non-Destructive Testing of Concrete

Comparing direct sound and coda measurement methods to analyze nonlinearities in ultrasonic sound speed response to distinguish concrete samples of different degradation grades

Master's thesis in Elektronisk Systemdesign og Innovasjon
Supervisor: Guillaume Dutilleux
Co-supervisor: Tonni Franke Johansen
August 2021

Norwegian University of Science and Technology
Faculty of Information Technology and Electrical Engineering
Department of Electronic Systems

NTNU
Norwegian University of
Science and Technology

,

NTNU

Kunnskap for en bedre verden

DEPARTMENT OF ELECTRONIC SYSTEMS

TFE4580 - ELECTRONIC SYSTEMS DESIGN AND INNOVATION, MASTER THESIS

Non-Destructive Testing of Concrete

Comparing direct sound and coda measurement methods to analyze nonlinearities in ultrasonic sound speed response to distinguish concrete samples of different degradation grades

Author:
Magnus Iben Holt
Supervisor:
Tonni Franke Johansen - SINTEF
Guillaume Dutilleux - NTNU

July, 2021

Foreword

Around Christmas 2020, I chose to switch subjects for my master thesis, from environmental acoustics to ultrasonics. At the time, I felt the work I had performed for my project thesis was sub-par and somewhat boring. Furthermore, as I anticipated yet another semester of Covid-19 restrictions, I figured that choosing a master thesis involving at least two fields of study in which I knew little about would provide me with so much difficult work, that I would not even notice the fact that I was stuck indoors. In addition, the prestige of writing a thesis for SINTEF, and the allure of a complex subject was tempting. The straw that broke the camels back in terms of deciding to switch subjects was the fact that my now ex-girlfriend's parents were specialized in the fields of concrete and ultrasonics respectively. As the prefix suggests, that particular motivation ultimately faded.

Being a student from Electronic Systems Design and Innovation, measurement techniques have been part of my academic endeavour the past five years. I like measuring stuff. I feel like I am fairly proficient at measuring stuff. What I have learned throughout my studies is that the first time you measure something, you are likely to fail to measure it well. Doing something badly is part of the process of learning. You analyze what you did, figure out what went wrong and improve.

With this thesis I did not have the opportunity to improve the technique. Due to the measurement equipment being damaged, the first measurements included in this thesis were taken six days before the original deadline. There was no time to improve. As you will discover whilst reading this thesis, the main source of error was discovered 48 hours before delivering the thesis, whilst writing the report. This source of error was, in an ideal world, supposed to be discovered months before. Just as the measurements presented in this thesis, in ideal world, would only be a step on the way to developing this thesis, and not the end product. Circumstances would not have it that way.

In addition to using this foreword as a chance to complain about the circumstances, I would like to thank those whom without their help, there would be no thesis.

I would like to thank, with the utmost sincerity, Sofia Godø and Bendik Bogfjellmo. They have been close friends, teachers, students and sources of healthy annoyance throughout my five years at NTNU.

I would like to thank Simen Tørnqvist, Brekke & Strand Akustikk AS, for supervising

me as a summer student. Without my experience as a working acoustician I would most likely have chosen a different profession.

I would like to thank Serhi Lovozy at SINTEF who literally worked through the night to be able to help me perform my measurements.

Lastly, I would like thank Tonni Franke Johansen, for believing in my ability to provide a valuable contribution to a project for which I had very little background qualifications. I hope I did not disappoint to much.

If we knew what we were doing
it would not have been called
research,
would it?

ALBERT EINSTEIN

Sammendrag

Målinger av variasjonen i ultrasonisk lydhastighet i betong, som funksjon av påtrykt tøyning ble foretatt 17. Juni 2021, ved SINTEF formasjonsfysikk. Betongprøvene var plassert i en kompresjonsramme med kompresjon på $28KN$ og påtrykt et varierende tøyningsfelt på maksimalet $\pm 1.5\mu\sigma$. Målet var å skille responsen betongprøver av ulik deformasjonsgrad ga under varierende tøyning. Oppgaven presenterer to ulike målemetoder brukt for å forsøke å observere de ulike responsene. En metode benytter seg av ultralydsignalets direkte transmisjon, mens den andre metoden benytter et tidsvindu som er 10 ganger større enn den første, og analyserer ultralydsignalets coda. De oppnådde resultatene var ikke tilfredsstillende. Et databehandlingsproblem forårsaket store avvik, og ble ikke oppdaget før det var for sent til å rette opp feilen. Målingene viser dog at metoden som benytter signalcodaen i analysen er mer lovende for videre utvikling enn metoden som benytter den direkte transmisjonen alene.

Abstract

Measurements of the varying ultrasonic sound speed in concrete as a function of imposed strain were performed June 17th 2021. The concrete samples were placed in a compressive frame with a confining pressure of $28KN$ and subjected to an additional varying strain, resulting in a maximum additional strain of $\pm 1.5\mu\sigma$. The aim was to differentiate the response between concrete samples of different degradation grades, and to compare the efficacy of two different measurement techniques to highlight these differences. One method utilized the direct ultrasonic signal, observing a strain field considered constant throughout the transmission. The second method utilized a time window 10 times larger, analyzing the signal coda. The results were in and of themselves unreliable, in large part to due a signal alignment error in the analysis discovered too close to the deadline to correct for. However, the research performed suggests that further development efforts should focus on honing the coda analysis technique.

Contents

Chapter 1

Introduction

1.1 Motivation

Concrete is one of the most important materials in the world. Whenever large structures are built, concrete is more than likely to be the load bearing material. Bridges, dams, stadiums and tall buildings are are examples of such structures that depend on the structural integrity of concrete. When this integrity fails however, the calamities are proportional to the size and function of the structure. When dams burst, rivers flood. When bridges collapse, we may consider ourselves lucky if the only consequence is a disrupted road network. When stadiums collapse, or tall buildings inside cities fall, people die. The degree to which concrete as a material is depended on for critical material tasks can not be overstated.

Far from being a modern invention, uses of concrete are found in Greek buildings dating back to Homeric times (1200-800 BC) [1]. Furthermore, Romans used concrete for many of their famous buildings. The Pantheon is still the worlds largest unsupported concrete dome, almost 1900 years after its completion. There are a vast number of Roman-built concrete structures built that stand without need of rehabilitation more than 2000 years after their construction.

Such durability can not be found in most modern applications of concrete. A horrendous example of quick degradation is the concrete used in the Stavanger Concert Hall. For decorative reasons, red and clear glass was mixed into the concrete. The building was completed in 2012, and won the Norwegian Concrete Element Associations prize for concrete structures. Nine years later the concrete showed such signs of degradation that it was in need of rehabilitation [2]. Fortunately this is not representative for most of modern concrete, but it serves as an example of how durability often must give way for other concerns. Bearing in mind that concrete is a material which serves critical tasks in the modern world, and the fact that modern concrete is seldom built with the same durability as in ancient times, effective methods of inspection must be developed. Furthermore,

concrete is a material in which cracks and deformities may not be visible on the surface.

Based on previous work, in particular by Riviere et. al. 2013 [11], and research conducted at SINTEF, this thesis presents a comparison between two methods of differentiating concrete of different degrees of degradation. Far from being field-ready, the research conducted is part of an effort to explore how elastic non-linearities can be utilized to assess the integrity of a concrete sample. This line of research may lead to effective methods of Non-Destructive Testing (NDT), with respect to both time consumption and accuracy. Should this line of research ultimately prove to be sufficiently useful, the most likely application may be bridges.

The need for more effective inspection-methods for bridges is dire. According to the United-States Infrastructure report card. 42% of American bridges are more than 50 years old, and 7.5% are considered structurally deficient [3]. These bridges support on average 178 million trips every day. In Norway, Statens Vegvesen is responsible for the inspection of Norwegian bridges. In 2017, Verdens Gang reported that regulations regarding inspection and rehabilitation of these bridges were violated for approximately 50% of Norwegian bridges [4]. Statens Vegvesen responded that they lack the capacity and the resources to fulfill the requirements. In the same report, journalists revealed that out of the 16971 bridges on main roads (riks- and fylkesvei), 1087 had large or critical damages [4]. Granting that there is a lack of capacity and resources, one of many contributions that can be made to ensure proper inspection of a larger number of these bridges, is the development of more effective test methods. Although the work presented here is far from being ready for field application, its motivation is to be a contribution to the research needed in order to invent new and more effective test methods.

1.2 Problem specification

This thesis presents a method attempting to differentiate concrete samples of different degradation states, by method of analyzing the nonlinearities in the Dynamo Acoustic-Elasticity (DAE). The aim of the project is to develop a method through which the nonlinear response can be observed using the available equipment. Specifically, the aim is to compare the information that is possible to obtain about the elasticity response when analyzing a directly received ultrasonic pulse transmitted through a concrete sample under dynamic stress, with the response found when analyzing the coda of a similar signal. The thesis provides the theoretical background from which this method was developed, and observes the results that were obtained through the application of the method. It is however the measurement technique itself that is the main point of examination. Neither being a material science thesis, nor a physics dissertation, this project should be viewed as an applied acoustic measurements endeavour. The discussion will centre around whether or not the technique seems to be able to provide a method of studying the elastic nonlinearities exhibited by concrete and will not delve deeply into explaining the phenomenon. An attempt was made to provide a protocol through which scientists at SINTEF could study

this more in-depth.

Chapter 2

Theoretical background

The following chapter provides the theoretical foundation on which the measurement techniques studied in this thesis stands. The measurement protocol borrows heavily from in particular two publications [11] [9]. Additionally, as this is a thesis in Acoustics, little to no prior knowledge in the material properties of concrete is presumed. The signal processing knowledge utilized is on the other hand presumed to be known by the reader, and its theoretical basis will not be outlined in this chapter, but rather described as implemented in the Methods chapter.

2.1 Concrete material composition

Concrete is a composite-material based upon mixing aggregate ($60\% - 80\%$), cement ($7\% - 15\%$), water and in some cases further additives ($< 2\%$) [5]. There are countless variations that can be made using these basic components in different ratios, and of different types. After mixing the components, the concrete cures (hardens) over time and settles into a durable material with a high compressive strength. However, in order to compensate for the lack of tensile strength, concrete may be reinforced with steel or other materials with high tensile strength.

The aggregates are usually sand or crushed rocks of varying sizes. Differently sized aggregates provide different properties for the concrete. By increasing the aggregate size, the compressive strength increases. There is also an reduction in deformation, as well as an increased Young's modulus and unit weight. The trade-off is a reduction in tensile strength. By increasing the maximum grain size to $120 - 180mm$ there is a reduction of $30\% - 50\%$ in tensile strength compared to concrete with a maximum granular size of $20mm$ [6].

The cement serves and the binding agent in the concrete mix and affects several aspects of the concrete in combination with the water content. The workability of the concrete is

heavily affected by the cement type and the Water/Cement (W/C) - ratio. By increasing the W/C-ratio, the concrete becomes more readily malleable and easier to mix. However, by increasing the W/C-ratio there is subsequent reduction in its compressive strength [7]. Although increasing the relative amount of cement in the concrete mix may lead to a reduction in durability [7], there is also work showing that an increased W/C ratio may lead to increased degradation as a result of increased porosity [8].

2.2 Elastic and acoustic properties

Under stress, materials undergo elastic or plastic deformation to some degree. Elastic deformation occurs when the material under stress returns to its original shape and size after the stress is removed. Under plastic deformation, the material is permanently deformed after stress is removed. The elastic property of a material is quantified as Young's modulus E [Pa]. Different materials will have different yield points, the point where additional stress becomes plastic. Beneath the yield point deformation is elastic, yet this elastic deformation is not linear for all materials and all stresses. There are several models of elastic responses to stress in materials. The simplest, linear representation of elasticity treats that can be applied to concrete treat the material as a spring, following Hooke's law [9].

$$\sigma = M \cdot \epsilon \tag{2.1}$$

where σ denotes stress, M is the elastic modulus and ϵ is the strain. The strain of the material under stress is a dimensionless quantity defined as [10]

$$\epsilon = \frac{\delta}{L} \tag{2.2}$$

where δ is the deformation and L is the length of the deformed material along the axis of deformation.

Hooke's Law (eq: 2.1) provides a fully linear relationship between the strain and the applied stress. However, as outlined by Stroisz [9], rock-like materials (such as concrete) does not exhibit linear stress-strain relations. A wide range of experiments show the nonlinear elastic behaviour in rocks and rock-like materials. Particularly relevant for this project is the work performed by Riviere et. al. [11] as will later be further explored in the method-specific theory section,

In order to account for the nonlinear elastic properties, further terms must be added to Hooke's law. The following equation expresses a stress-strain relation for a perfect

nonlinear response [9]

$$\sigma(\epsilon) = M \cdot (\epsilon + \beta \cdot \epsilon^2 + \delta \cdot \epsilon^3 + ...) \tag{2.3}$$

where β and δ are nonlinear coefficients. The response described by this expression shows is the simplest nonlinear response, and shows no hysteretic or conditioning (dependence on stress history) behaviour. Rocks do however often exhibit hysteretic stress-strain behaviour, where the loading and unloading process do not follow the same stress-strain curve. In order to take stress history into account in the nonlinear model the addition term $\hat{\alpha}$, [9]

$$\sigma(\epsilon, \dot{\epsilon}) = M \cdot (\epsilon + \beta \cdot \epsilon^2 + \delta \cdot \epsilon^3 + ...) + \hat{\alpha}[\epsilon, sign(\dot{\epsilon}] \tag{2.4}$$

where $\dot{\epsilon}$ denotes the strain rate $\epsilon = \partial\epsilon/\partial t$ [9]. This model applies well to non-perfectly elastic materials. That is materials where the hysteretic response loop is closed, i.e. where the material does not undergo plastic deformation. As will be further detailed, this elastic behaviour is observed by Riviere et. al [11] in Berea sandstone by relating the change in ultrasonic sound speed to the elasticity. Sound speed and elasticity is classically related through the following equation [10]

$$c = \sqrt{\frac{E}{\rho}} \tag{2.5}$$

where ρ is the density of the material. Figure 2.1 contains the curves corresponding to each of the previously described elasticity models.

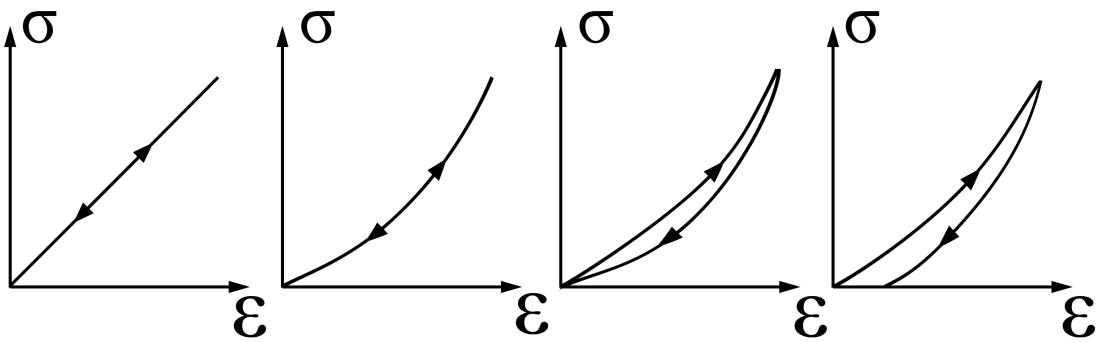

Figure 2.1: Stress/Strain relations. Reading from left to right, the curves describe linear elastic response, perfect nonlinear elastic response, non-perfect nonlinear elastic response with hysteresis, non-perfect nonlinear elastic response with hysteresis and partial plastic deformation. Figure recreated from [9].

2.3 Static- and Dynamo-Acoustic Elasticity

There are two main ways of studying the elastic response of rock-like materials acoustically. In this project DAE was used. However, static measurements are worth mentioning, as in work performed at SINTEF using static measurements has informed on of the two measurement methods used. In static elasticity response measurements, the sample is placed under static stress and sound speed recorded using ultrasonics for various stress amplitudes in both the loading and unloading cycle. By using the static technique, it is possible obtain to very fine-grained data for the stress-strain relation, utilize averaging of an arbitrary amount of pulses to achieve a higher signal-to-noise ratio (SNR), as well as recording both the direct pulse and a long coda. Research performed at SINTEF prior to this project using the static approach seemed to indicate that the signal coda may contain as much, if not more, interesting data as the direct pulse. This research is still on-going, and is not part of this thesis in and of it self. It did however influence the measurements taken during this project due to the suspicion that the signal coda contained valuable information on the elasticity response. In contrast to these static measurement, the measurements described in this thesis were of the dynamic type. When performing DAE measurements, the ultrasonic sound speed is measured while the sample is under continuously varying stress. Obtaining finely grained data is a somewhat more difficult task, as one needs to combine both precise pulse-excitation and simultaneous recording of both ultrasonics and deformation in the sample. This type of measurement is part of what is in general called the pump-probe method [11].

2.3.1 Pump-probe method

Pump-probe methods have been used to study nonlinear acoustics from as early as the 1950s [11]. The method is performed by utilizing two dynamic fields, one low-frequency field (LF), the pump, and one high-frequency field (HF), the probe. The pump is used to change the strain field in the sample in a controlled manner, while the probe field is used to measure the characteristics of the sample at different strain levels. By relating stress, strain and sound speed using the aforementioned equations, the nonlinearities in the elastic response curve may be analyzed. The pump-probe method is widely used, and can be implemented both as in the case of this project, with the LF field applied along one axis of the sample, and the HF field applied across this axis normally. It may also be applied uniaxially as a combined signal pulse, as in the case of the SURF-technique utilized in the doctoral thesis by Stroisz [9].

2.3.2 SURF

The Second order UltRasound Field technique (SURF) is an adaption of previous dual-frequency imaging techniques applied to biological materials[9]. The SURF uses one

pulse containing both LF and HF components where the pump-pulse amplitude is very large. By ensuring a sufficiently large amplitude of the pump-component, the material changing compressive and tensile states perturb the LF pulse, but only shifts the HF pulse in time relative to the LF pulse. By simultaneously transmitting both pulses, the HF pulse travels through the sample under measurement along with the LF pulse and experiences the effects of the pump pulse along the transmission path. When applying the SURF technique, the frequency ratio between the HF and LF pulses should not exceed $1/7$. This is necessary to ensure that the probe pulse experiences a sufficiently small part of the period of the pump pulse [9]. The stress-dependence of the wave-velocity is modeled as the sum of the linear elastic sound speed component c_0 and the nonlinear stress-dependent component and is calculated as follows [9]

$$c(\sigma) \approx c_0 + \left.\frac{\delta c}{\delta \sigma}\right|_{\sigma=\sigma_0} \cdot \Delta\sigma \tag{2.6}$$

This is by no means an extensive explanation of the SURF technique, but contains the knowledge that was used to influence the methodology applied in this project.

2.3.3 Delay calculation

The delay is calculated by using cross correlation, as described in the following equation.

$$C(\tau_j, t_j) = \int_0^\infty s(t - t_0)s(t + \tau - t_j)dt \tag{2.7}$$

where τ_j is the shift in time of flight. This time is interpolated by fitting a second degree polynomial to the peak of the cross-correlation function and its two adjacent points. By considering the cross correlation maximum to be located at $x = 0$, second degree polynomial coefficients can be determined through the following expressions:

$$\begin{aligned} f(x) &= ax^2 + bx + c \\ a &= \frac{f(1) + f(-1)}{2} - f(2) \\ c &= f(0) \\ b &= \frac{f(1) - f(-1)}{2} \end{aligned}$$

The location of the peak of the calculated second degree polynomial will then correspond to fraction of one sample, that is added to the overall delay. The peak is calculated as;

$$x = -\frac{b}{2a} \tag{2.8}$$

The relative change in sound speed is calculated as

$$\frac{\Delta c}{c} = -\frac{\Delta \tau}{t_0} \tag{2.9}$$

where $\Delta\tau$ is the delay found through cross-correlation and polynomial interpolation and t_0 is the time of flight as the reference pulse [11].

Chapter 3

Method and materials

3.1 Measurement setup

The measurement setup used is an adapted version of a setup used in previous work [11], and is a pump-probe type measurement. It utilizes a $50KN$ compression frame and a piezoelectric vibration element to generate the strain field, and ultrasonic transmission wave probing. An oscilloscope used to collect the relevant signal data. Figure 3.1 shows the measurement setup as a diagram. Figure 3.2 is a picture taken of the measurement setup in a $10KN$ frame that was used for testing the measurement equipment. The signal generator and power amplifier used as input to the ultrasonic transducer used as emitter is visible in the bottom left corner. The conditioning amplifier in the bottom right corner is used for the received ultrasonic signal. The signal generator used to generate the vibration signal for the piezoelectric element is visible in the top right corner. The power amplifier used for this signal is just outside the frame, on top of the signal generator. The oscilloscope and the conditioning amplifier used to prepare the accelerometer signals are visible in the low-middle section of the frame. Figure 3.3 shows a close-up of the non-degraded concrete sample in the compression stack. The ultrasonic transducers are held in place by a clamp, with a coupling membrane between the transducers and the sample. An accelerometer was placed both on the vibration element and on the steel base-plate. The measurements were taken June 17th 2021 at the SINTEF Formation Physics lab in Trondheim.

3.1.1 Samples and resonance

Three concrete samples of different degradation grade was used. One sample was in pristine condition and the other two were artificially aged to different degrees. The samples were provided by SINTEF, and the exact process of degradation is unknown to the author. All samples were of the same dimensions, with a base area of $49cm^2$

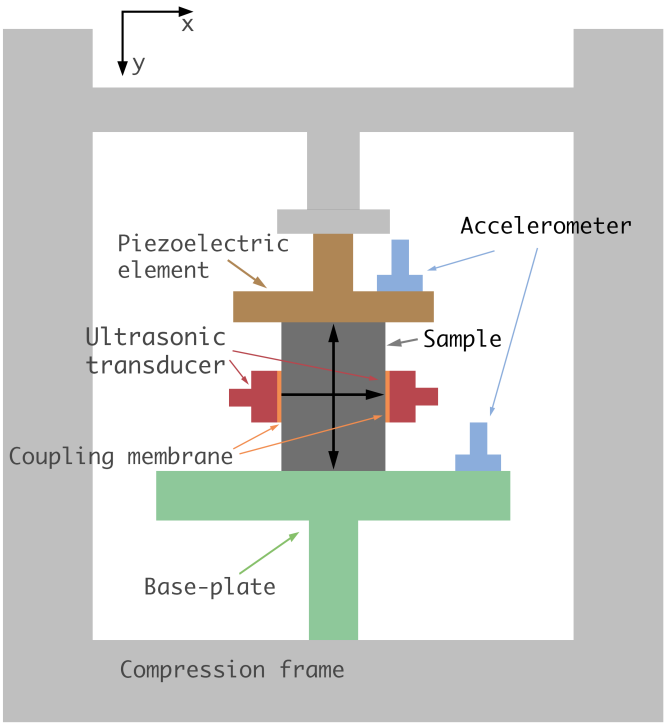

Figure 3.1: Figure depicting the measurement setup. Note that the positive y-axis is downward.

and a height of $10cm$. Under fixed-free boundary conditions, the samples would have a resonant frequency of $f_0 = c/4L \approx 8kHz$ along the dimension under vibration, The overall vibration system is however more convoluted than fixed-free boundary conditions can account for. The compression frame, the steel base-plate and the vibration element together combine with the sample under test to create a more involved mass-spring system. In this vibration system the concrete sample may be considered as a spring, by its lower relative stiffness compared to the steel base-plate, considered a mass. It was on the basis of this hypothesized that it was possible to achieve a significantly lower resonant frequency for the system under test.

3.1.2 Pump-field setup

Figure 3.4 shows a block-diagram of the signal path used to generate and measure the low-frequency pump field. A sine wave was generated by the signal generator and after amplification the piezoelectric element applies a varying stress field in the sample. Two accelerometers were used to record the vibrations present in the sample. One atop the vibration element, and one on the base plate. The accelerometer signals were filtered by the conditioning amplifier using a bandpass-filter with pass-band $10Hz - 22.4kHz$. The

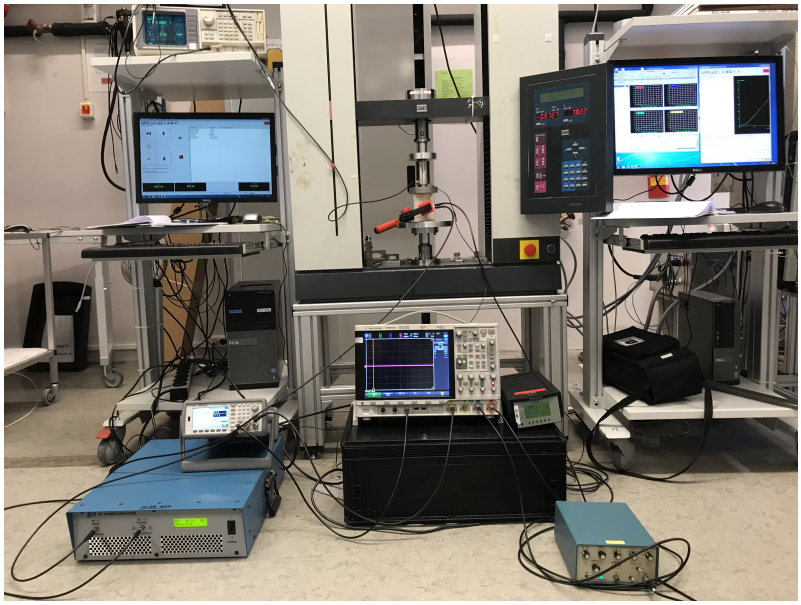

Figure 3.2: Image of the measurement setup used. The image is taken in the $10KN$ compression frame used while developing the method. The power amplifier for the vibration element is just outside the frame in the top left corner.

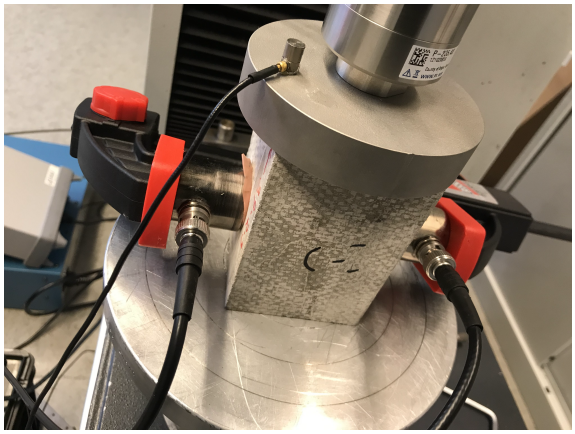

Figure 3.3: Close up image of the sample in the compression stack. The ultrasonic transducers are clamped to the sample, with a coupling MATERIAL in between the transducer and the sample. The vibration element is atop the sample, and a the sample stands on a steel base-plate. One accelerometer is mounted on top of the vibration element. The second accelerometer mounted on the base-plate is not visible in this image.

conditioned accelerometer er signals were recorded by the oscilloscope.

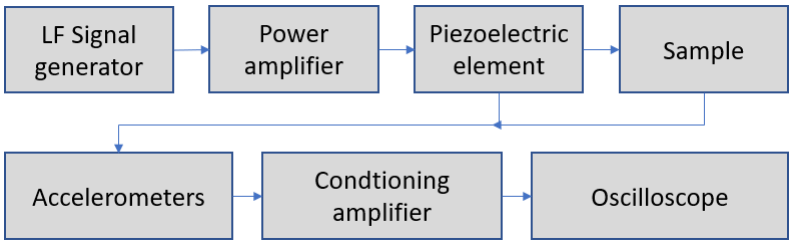

Figure 3.4: Block diagram of the signal path used for the pump field.

3.1.3 Probe-field setup

Figure 3.5 shows a block diagram of the probe field setup. A signal generator was used to provide the probe pulse, as well as trigger the oscilloscope data collection. The signal generator output was a 3 period sine wave-pulse with a frequency of $500kHz$ and an amplitude of $200mV_{pp}$. The signal generator output was recorded by the oscilloscope, in order to be able to estimate c_0. The subsequent power amplifier had a gain of $50dB$. After amplification, the probe signal was transmitted through the sample and received by the ultrasonic transducers clamped to the sample, with COUPLING MATERIAL between to ensure proper contact and power transmission. The received signal was amplified and filtered using a conditioning amplifier. A high-pass filter with a pass-frequency of $0.3MHz$ was used to reduce noise. Subsequently, the received probe-signal was recorded by the oscilloscope.

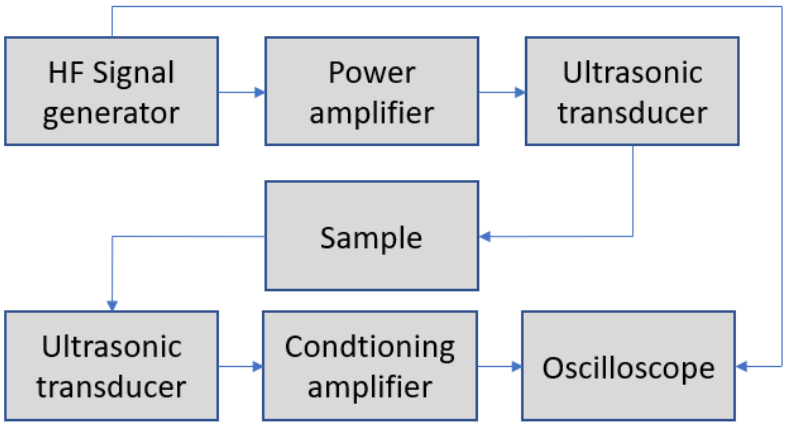

Figure 3.5: Block diagram of the signal path used for the probe field.

3.2 Measurement protocol

3.2.1 Measurement preparations

Three different types of measurements were performed for each sample, reference measurements, small time-window measurements applied to study the direct probe-pulse, and long-time window measurements designed to study the probe-signal coda. Before measurements could be performed, there were several steps of preparations that needed to be undertaken. As the oscilloscope used always recorded with the maximal sampling frequency possible, the amount of time windows recorded and the length of each window resulted in different sampling frequencies for the three types of measurement. In order to set the correct burst period to capture the desired phase-points of the vibration cycle, calculations were performed. In addition, a suitable probe-field had to be searched for.

3.2.1.1 Vibration frequency determination

In order to achieve the highest amount of strain possible in the sample, it was desirable to find resonance in the vibration system. The appropriate vibration frequency was found in a somewhat crude manner. By observing the amplitude difference between the top and bottom accelerometer, an attempt was made to tune the vibration signal to a frequency where the deformation would be as large as the system would allow. Bearing in mind that the actual deformation of the sample would the amplitude of the recorded difference differentiated twice by the jw-method, assuming harmonic behaviour. As the frequency increases, the deformation decreases, and with constraints on the power output to the vibration element, individual suitable frequencies were searched for in the $900Hz - 1.2kHz$ range for the three samples.

3.2.1.2 Burst period calculations

In order to find the correct burst period, several parameters were used as input to a MATLAB script. The main parameters considered were the length of the recorded time-frame, the sampling frequency, the vibration frequency, the amount of phase-points under consideration and the amount of repetitions desired for each phase point. Each phase point was to be recorded 15 times, a step taken to be able to average the resulting delay of each part of the compression-tension cycle, in order to eliminate noise and achieve a smaller confidence interval for each point. The burst period would need to correlate with the vibration frequency period in such a way that it hit the all the desired phase-points and subsequently repeated itself. If the number of total revolutions through the vibration cycle shared factors with the number of sampled degrees desired, the resulting recordings would not hit all the desired degrees, but rather repeatedly sample a fraction of the phase degrees. The following algorithm was developed to ensure this did not happen and acquire

the correct burst period.

```
%% Calculate period

minTotShotTime = degs * minDelay;

minRevs = ceil(minTotShotTime/vibPeriod); %minTotShotTime/period -->
    min # periods, ceil to be safe

revFac = factor(minRevs);
degFac = factor(degs);

while (sum(revFac.*ismember(revFac,degFac))>0) %minRevs cant share
    factors with degs so as to not repeat prematurely
    minRevs = minRevs +1;
    revFac = factor(minRevs);
end


trigPeriod = minRevs*vibPeriod/degs;

trigSamplePeriod = trigPeriod*fs; % #Samples between triggers
```

An example of how the calculated burst time provides sampling of each individual desired phase-point is included in Figure 3.6. In the example used, six phases are sampled for each vibration period, one phase-degree of each color is sampled. The parameters chosen for the exampled are different than the ones used in the measurements, in order to provide a better illustration of the concept. A (quite satisfying) animation of the process can be viewed or downloaded $here$. A figure proving that the process repeats itself the desired amount of times is provided in the appendix, with 15 repetitions.

3.2.2 Measurement procedure

Every measurement were performed such that there were 15 repetitions that could be averaged for each strain state. The full measurement protocol for each sample comprised of one set of 15 reference measurements, with a time-window of $350\mu s$. Each set of 15 measurements was saved. The reference measurements were conducted without varying stress. One set of 15 averaged measurements with 50 phase-degrees probed, with a time-window of $35\mu s$, and one set of 15 averaged measurements with 4 phase-degrees probed with a time-window of $350\mu s$. The preparation for, and execution of the measurement procedure was performed for one sample at a time. Firstly, the vibration frequency was determined. Subsequently, an arbitrarily long burst-period was chosen, and the reference measurements were taken. After the reference data was collected, and the oscilloscope armed for the set of 4×15 coda measurements, the oscilloscope sampling rate was recorded, and the appropriate burst-period calculated. Once gathered, the signal generator was set and measurements were taken for three different vibration amplitudes. Subsequently, the process was repeated fort the measurement sets of 15×50 direct

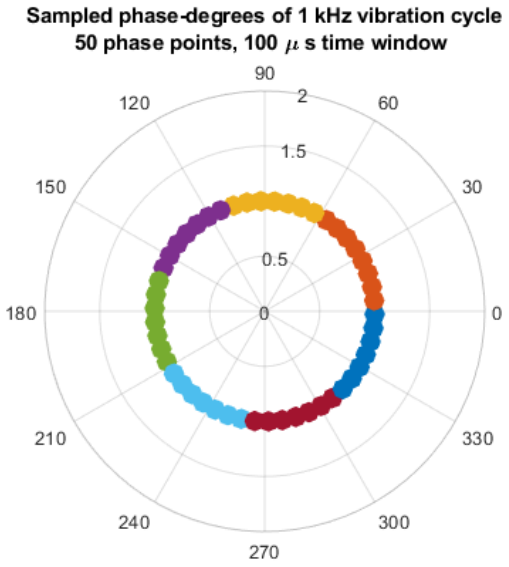

Figure 3.6: Example of how the burst-period algorithm provides a trigger period that allows for the sampling of the desired amount of phase points. The example used is for 50 desired phase points, with a $100\mu s$ time-window recorded each sampling, for a vibration frequency of $1000Hz$. One point of each color is sampled each period.

transmission measurements, with time-window $35\mu s$. This process was repeated for each of the three concrete samples.

Unfortunately, the file containing the reference measurement for the pristine concrete sample was corrupted. This was realized after the window of opportunity to redo the measurements had closed. In order to still produce results for this sample, a reference signal was calculated as the average of all sampled signals. This may be an appropriate reference, assuming perfectly elastic deformation, and that all phases of the deformation cycled were sampled equally. The equipment was available for a very limited time, as the piezoelectric actuator was in disrepair until June. Being a highly active lab, the availability of the compressive frame was also quite limited.

3.2.3 Post-Processing

The post-processing was performed in MATLAB. The saved .bin files containing each set of measurements are structured in such a way that the gathered $n \times 15$ segments are stored one channel after the other. The MATLAB script provided by the oscilloscope manufacturer proved was adapted to be able to read out all the measurement data in an efficient manner. Three data-structures were created for each sample, corresponding to the three vibration amplitudes. The data collected, accelerometer and ultrasonic data, was averaged for the corresponding phase-degrees. The accelerometer data was low-pass filtered, as there was a significant amount of high-frequency noise present. The

cut-off frequency was $1.5kHz$. As the reference measurements had a significantly higher sampling rate than the other measurements, the ultrasonic amplitudes were resampled using MATLAB's resample function. The coda measurements were resampled by a factor of $3570/926$ and the direct sound measurements were resampled by a factor of $3570/321$. After resampling, each averaged measurement were cross-correlated with the reference measurement. To achieve sub-sample resolution, a second degree polynomial was fitted to the cross-correlation maximum and its two adjacent points. The data was sorted by inversing the order in which the burst-period algorithm sampled phase-degrees. The arrays were then circularly shifted in order to obtain increasing and decreasing strain as the first and second half of the array.

The acceleration difference between the upper and lower accelerometer were taken as the true acceleration of the sample, and the strain field was assumed to be homogeneous throughout. The strain was then calculated as

$$\sigma = \frac{A_d}{Lw^2 s} \tag{3.1}$$

where $A_d = A_{top} - A_{bot}$ is the accelerometer difference between the top and bottom of the sample, L is the height of the sample, $w = 2\pi f_{vib}$ and s is the sensitivity of the accelerometer in V/ms^{-2}. The negative sign corresponding to $j^2 = -1$ cancels as the accelerometer gives a positive voltage when accelerating in the negative y - direction. Compressive strain is defined as positive.

For the coda measurements, the processing was performed both for the entire measurement frame, as well as for three smaller windows in the signal coda. An early, middle and late coda analysis was performed.

3.3 Equipment list

Equipment	Manufacturer	Model	Serial number
Oscilloscope	Agilent	DSO-x 4024A	MY53110131
HF-signal generator	Agilent	33500B	MY2200356
LF-signal generator	Stanford R.S.	SR850	87361
HF-power amplifier	PI	RF power amplifier	-
LF-power amplifier	PI	E-471.20	110024556
HF-conditioning amplifier	Panametrics	5055PR	697
Acc. conditioning amplifier	Brüel & Kjær	NEXUS	CB-2116
Accelerometer x2	Brüel & Kjær	4344S	-
Ultrasonic transducer x2	Olympus	V101	-
Piezoelectric actuator	PI	P-235.40	121020824
Clamp	-	-	-
Laptop	Dell	XPS 15 9570	-

Chapter 4

Results

The following chapter contains figures illustrating the results gathered from both of the measurement methods, for each sample and vibration input voltage. The measurements based on the analyzing the direct sound are presented first, followed by the results of the coda measurements.

4.1 Direct sound measurements

4.1.1 Pristine sample

4.1.1.1 Vibration behaviour

Figure 4.1 contains the average sampled acceleration of the top accelerometer, compared to the average sampled difference between the accelerometer mounted atop the sample and the accelerometer mounted on the base plate for each of the input voltages used for the pristine concrete sample. Ideally, there would have been no acceleration at the base plate, and the acceleration difference equal to the acceleration at the top of the sample. This is clearly not the case, and there is significant movement present in the base-plate. In addition, in the case of $0.15V$ vibration voltage input, the sampled points do not follow the intended behaviour. The increasing and decreasing strain classification is performed by sorting the measurement sets such that the first 25 samples of Figure 4.1 are increasing, and the last 25 are decreasing. The consequence of this is that some points at the beginning and end of a increasing/decreasing strain cycle may be inaccurately classified.

Figure 4.2 depicts four series of 15 sampled supposed equal strain repetitions. Each color represents what was supposed to be equal strain levels. As can be seen from the figure, the intended equal strain repetitions are not equal. In the case of the $0.15V$ vibration input voltage, Figure 4.2 shows that the strain field likely was sampled at the intended amount

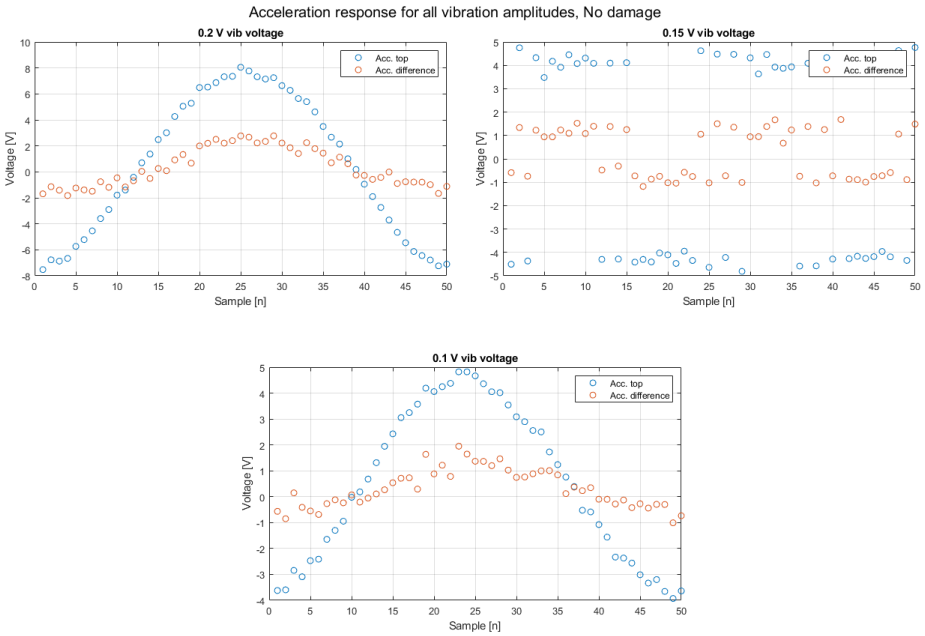

Figure 4.1: The average acceleration of the top accelerometer and the average accelerometer difference for the sample with no damage.

of phases, and suggests that the four roughly equal phases depicted in figure 4.1 may be a result of a sorting error. As the scripts used to analyze the measurements of the same type are equal, apart from changing the input data, it is unclear why this sorting problem arose. For the remaining input vibration voltages, Figure 4.2 shows that the precise strain field phase-sampling approach applied, did not translate well from theory to practice. The ideal case would have been for this plot to contain straight lines of points along one strain level for each set of plotted points.

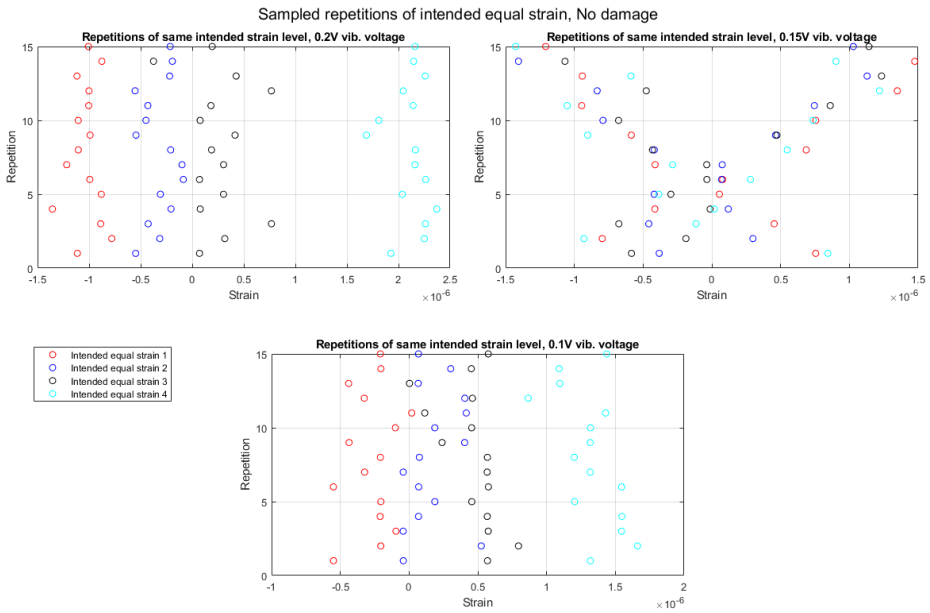

Figure 4.2: Repetitions for averaging of supposed equal strain for the three vibration voltage inputs. Figure clearly shows that there is a large discrepancy between samples. In the ideal case, all repetitions would fall on a straight line at one point on the strain axis. Concrete sample with no damage.

4.1.1.2 DAE - results

Figure 4.3 depicts the delays as percentage of reference transmission time, plotted against the strain averaged across the 15 repetitions of each intended equal strain point. The difference in delay between the fastest and slowest sampled transmission times are in a realistic range compared to previous research [11], being around a tenth of one percent.

However, the delays are much larger than what can be expected to be correct, as more than 30% reduction in sound speed compared to the reference is very unlikely. The difference between delays seems much more reasonable than the delays themselves. It should also be noted that as the file containing the reference measurements for the undamaged sample was corrupted, the reference signal used was the average of all sampled time windows. The plot for the $0.15V$ vibration input voltage is scrambled and contains no useful information, just as it is in Figure 4.1. A figure of all the sampled points are included in the appendix.

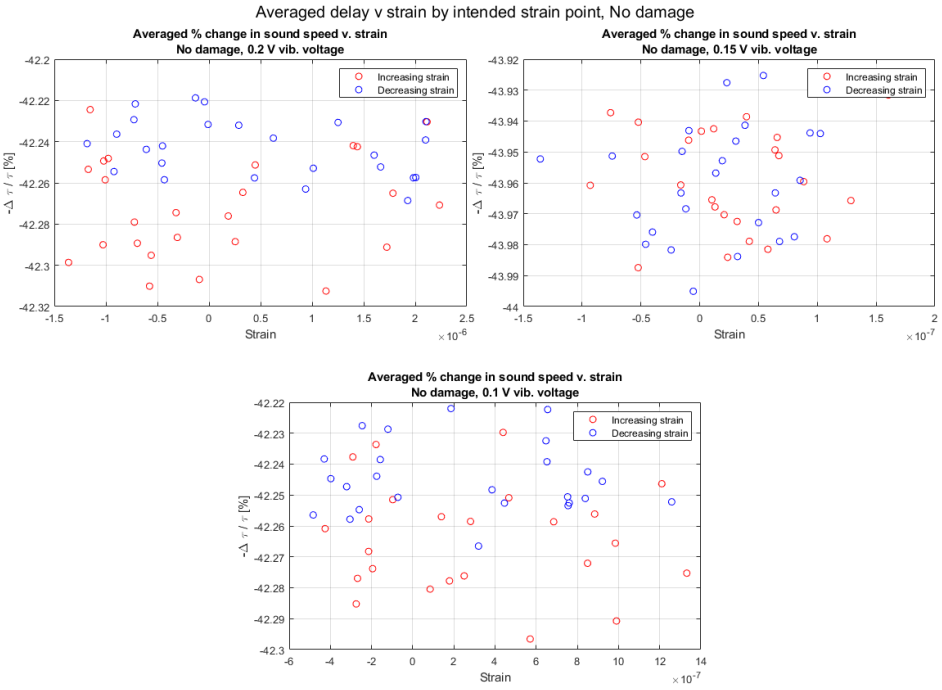

Figure 4.3: Average delays in percent relative to the reference transmission time sampled plotted against corresponding strain for the sample with no damage. 15 samples of the same intended strain.

4.1.2 Medium damaged sample

4.1.2.1 Vibration behaviour

Figure 4.1 shows the average acceleration sampled at the top of the concrete sample with medium damage, compared to the acceleration difference between the top and bottom accelerometer. There is a phase difference between the the two plotted measures, in particular for the largest vibration input voltage. There also seems to be some distortion, as the decreasing part of the curve is steeper than the increasing part. In contrast to the acceleration of the undamaged sample shown in Figure 4.1, there seems to be less movement in the base-plate, as the difference between the two plotted measures are smaller for the concrete sample of medium damage.

Figure 4.2 depicts the intended repetitions of equal strain for the concrete sample of medium damage. Just as for the undamaged sample, there is noticeable spread in these plots. The ideal case would have been that all 15 repetitions sampled the same strain, which would have been represented by a straight line.

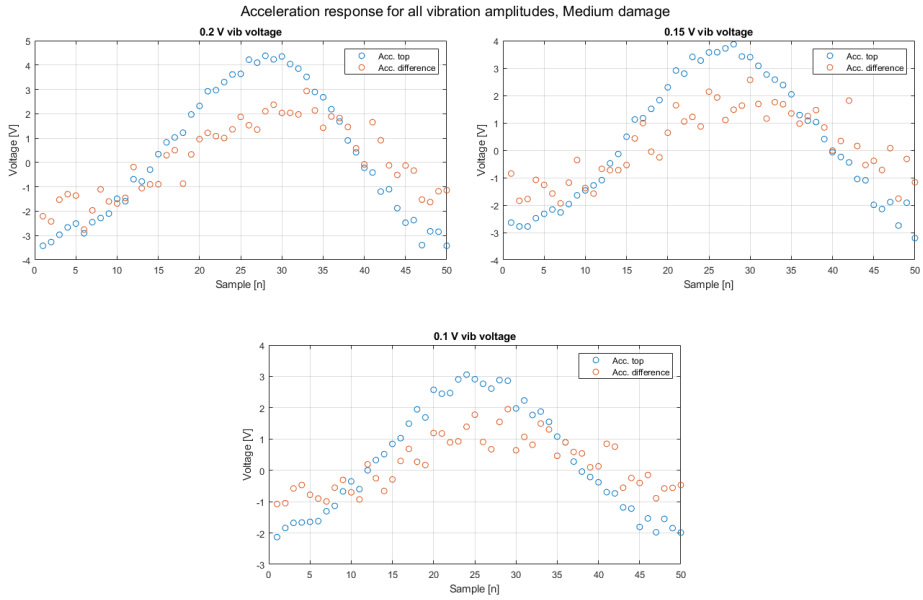

Figure 4.4: The average acceleration of the top accelerometer and the average accelerometer difference for the sample with medium damage.

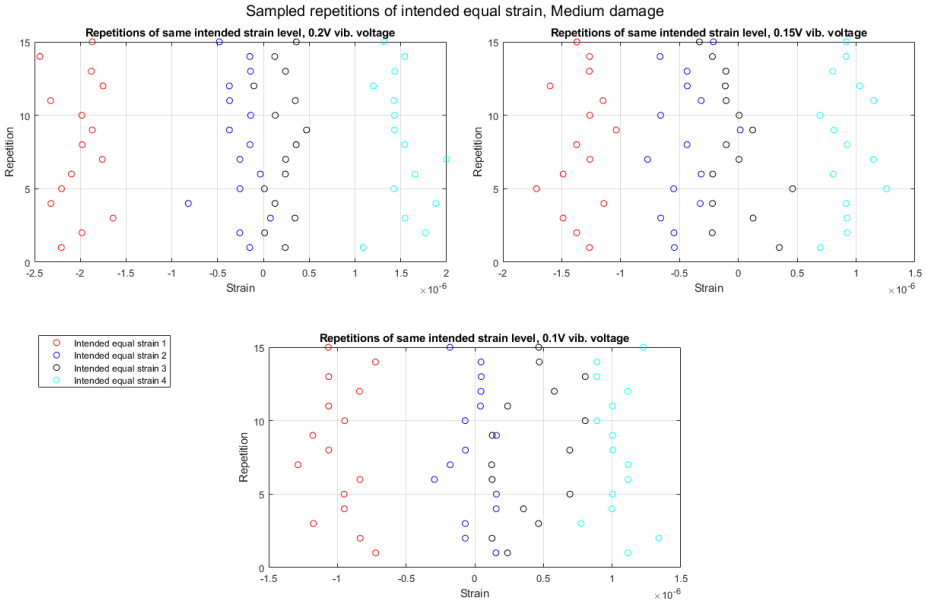

Figure 4.5: Repetitions for averaging of supposed equal strain for the three vibration voltage inputs. Figure clearly shows that there is a large discrepancy between samples. In the ideal case, all repetitions would fall on a straight line at one point on the strain axis. Concrete sample with medium damage.

4.1.2.2 DAE - results

Figure 4.6 depicts the average delays in percent relative to the reference transmission time plotted against the corresponding strain. 15 repetitions of each intended strain point is sampled. From Figure 4.6 we can observe that the sound speed increases (delay decreases) as compressive strain increases, and subsequently decreases as the the strain decreases. This behaviour becomes decreasingly visible as the vibration voltage input decreases. A figure of all the sampled points is included in the appendix.

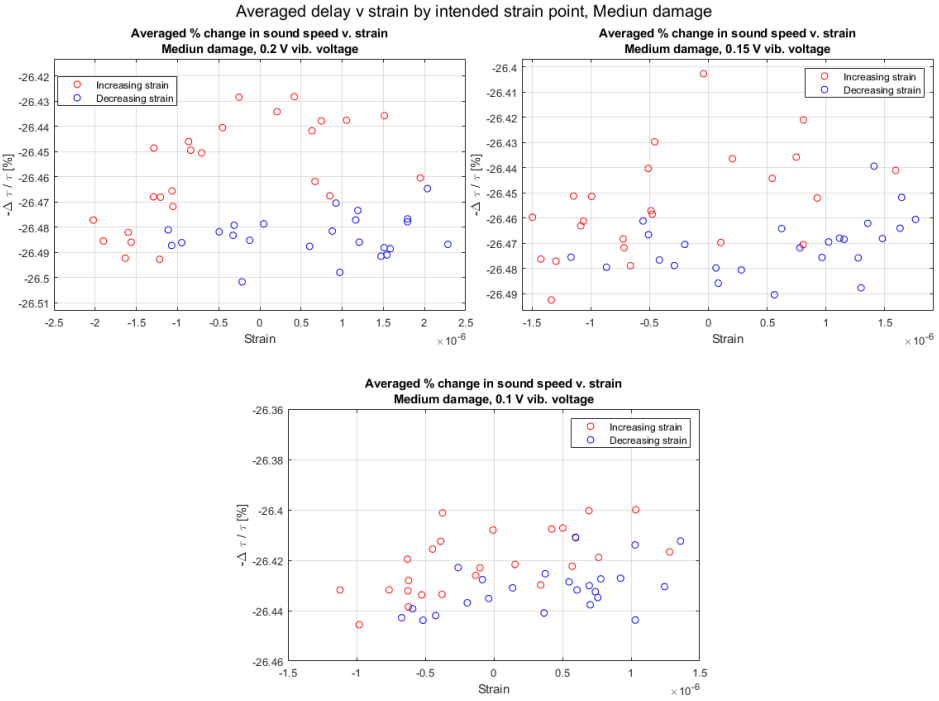

Figure 4.6: Average delays in percent relative to the reference transmission time sampled plotted against corresponding strain for the sample with medium damage. 15 samples of the same intended strain.

4.1.3 Severely damaged sample

4.1.3.1 Vibration behaviour

The severely damaged concrete sample showed vibrational behaviour comparable to the sample with no damage, as can be seen by comparing Figure 4.7 and Figure 4.1. There is large movement in the base-plate as the difference between the top and bottom accelerometer is significantly smaller than for the concrete sample with medium damage. There is no phase shift or apparent distortion present in the vibrational behaviour exhibited by the sample with severe damage.

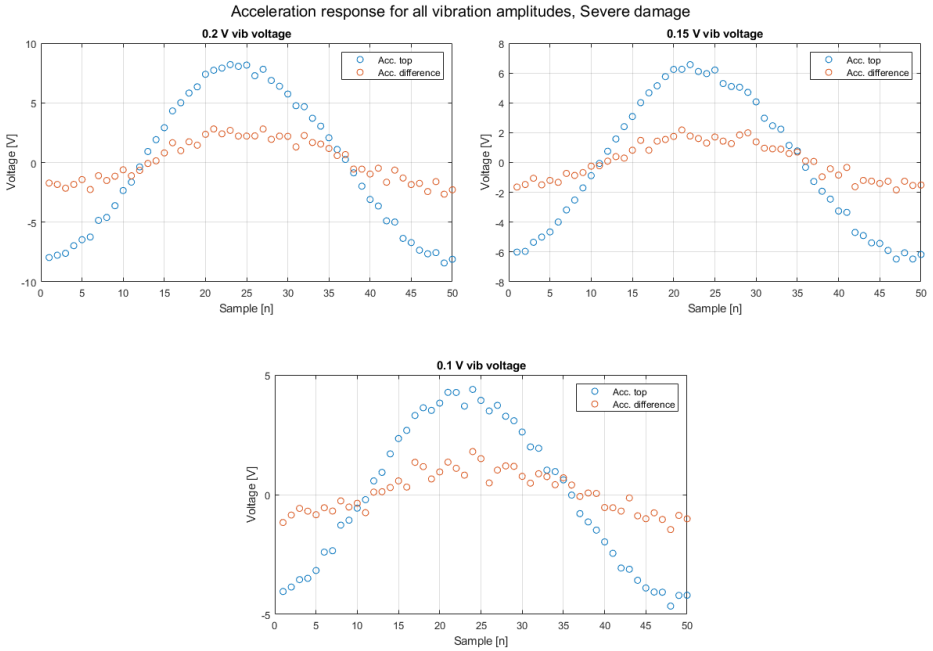

Figure 4.7: The average acceleration of the top accelerometer and the average accelerometer difference for the sample with severe damage.

Figure 4.8 depicts four sets of intended equal strain repetitions. Just as for the previously described samples, the intended equal strain points show significant variance.

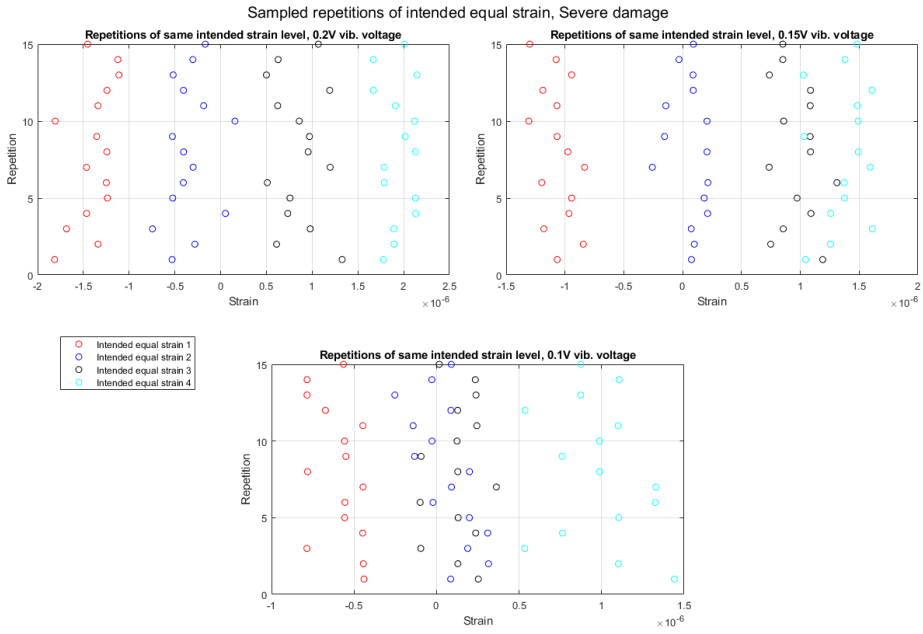

Figure 4.8: Repetitions for averaging of supposed equal strain for the three vibration voltage inputs. Figure clearly shows that there is a large discrepancy between samples. In the ideal case, all repetitions would fall on a straight line at one point on the strain axis. Concrete sample with severe damage.

4.1.3.2 DAE - results

Figure 4.9 depicts the averaged delays as percentage of the reference transmission time plotted against the corresponding strain for the severely damaged concrete sample. Similarly to the concrete sample with no damage, depicted in Figure 4.3, it is difficult to discern any clear pattern in these plots. Just as for all the previously described average delay figures, the magnitude of the delays seem to be far from realistic. The difference between the largest and smallest delay seems however to be much more realistic.

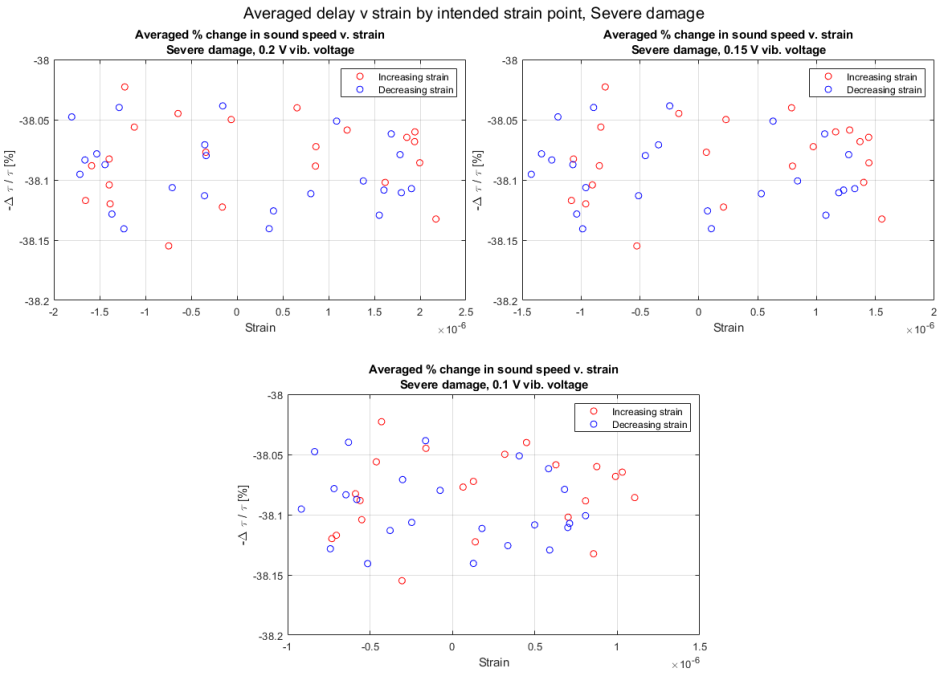

Figure 4.9: Average delays sampled plotted against corresponding strain for the sample with no damage. 15 samples of the same intended strain.

4.2 Coda Measurements

4.2.1 Pristine sample

4.2.1.1 Vibration behaviour

Figure 4.10 includes plots of all the repetitions of each part of strain cycle used for the coda analysis for the concrete sample with no damage, when a vibration voltage input of $0.2V$ was used. In blue, the ultrasonic amplitude is plotted, the accelerometer difference in red, the top accelerometer in green and the base-plate accelerometer in magenta. We can observe that there is little to no phase difference between the two accelerometer signals. In addition, in the first parts of the increasing and decreasing strain cycles, the acceleration seems to flatten towards the end of the window. This behaviour may be the result of low-pass filtering, as the acceleration should be continuously increasing/decreasing when crossing $0V$. The measurements taken of the undamaged concrete sample with a vibration voltage input of $0.15V$ and $0.1V$ captured the vibration signal with an offset compared to the measurements with $0.2V$ input. As can be seen from Figure A.4 and Figure A.5 in the appendix, the acceleration does not flatten around $0V$, but it does flatten towards the end of each window.

4.2.1.2 DAE - results

Figure 4.11 shows a plot of the delay as percentage of the reference transmission time plotted as the average strain for each of the three vibration voltage inputs. Each line corresponds to one of the subplots in Figure 4.10. The three points on each line corresponds to an early, middle and late window applied to the signal. The first window from $0\mu s - 100\mu s$, the second from, $100\mu s - 200\mu s$ and the third from $200\mu - 350\mu s$. The strain is averaged for the applied window. As the measurements taken with vibration voltage input of $0.2V$ had a offset compared to the two others, it shows different parts of the strain cycle. As was the case with the direct sound measurements, the magnitude of the delays seems to be larger than what would be expected. What can be observed from these plots however, in particular from the plot from measurements taken with $0.1V$ vibration voltage input, is changes in sound speed consistent with the hysteresis model [11]. Furthermore, it can be noted that the scripts analyzing the three different measurement sets, are completely equal, and it is unclear why the delays found with $0.2V$ input voltage, and the measurements for the concrete sample with medium damage (as will be shown) is in a much more realistic region than the rest of the measurements.

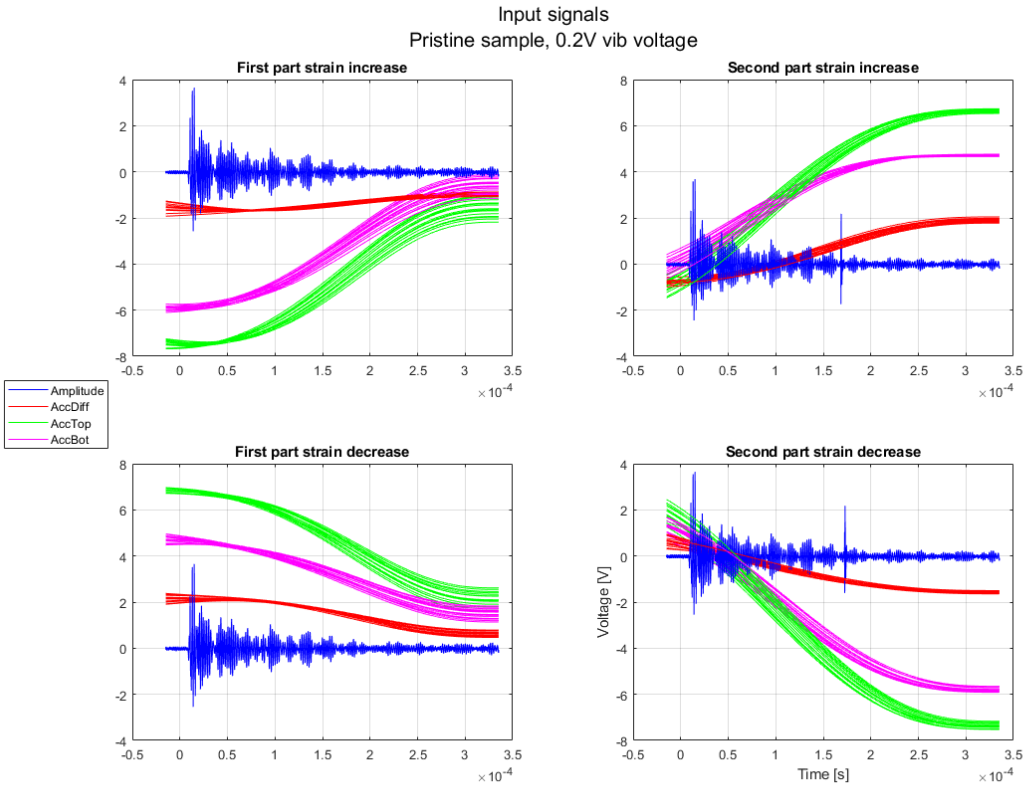

Figure 4.10: All gathered signals from coda measurements of the concrete sample with no damage, for vibration voltage input of $0.2V$. The plots are divided into the first and second parts of the increasing and decreasing parts of the strain cycle.

4.2.2 Medium damaged sample

4.2.2.1 Vibration behaviour

Figure 4.12 shows all the signals gathered of the concrete sample with medium damage, for vibration voltage input of $0.2V$. Figures A.6 and **??** show the same plots for vibration voltage input of $0.15V$ and $0.1V$. As opposed to the measurements of the concrete sample with no damage, the sampled time windows seem to gather more or less the same part of the strain cycle for all vibration voltage inputs. Furthermore, there is a phase difference between the acceleration at the top and the bottom of sample, which was visible in the same manner for the direct sound measurements of the same concrete sample. We can observe a flattening of the acceleration signals toward the of the sampled window, similar to the flattening present for the sample with no damage.

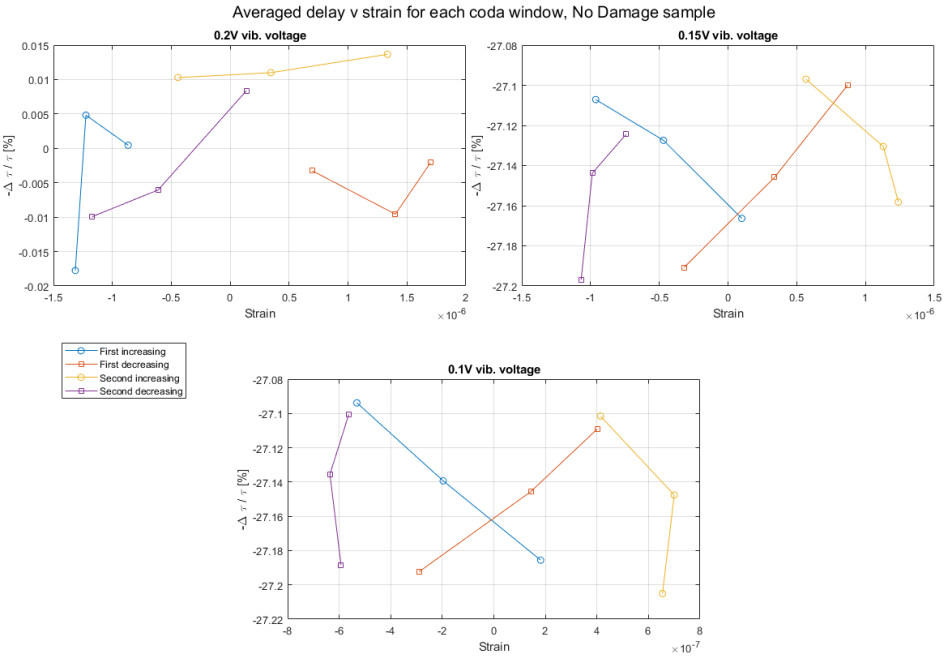

Figure 4.11: Delay as percentage of the reference transmission time plotted as the function of average strain for each of the three vibration voltage inputs. Each line corresponds to one of the the four subplots in Figure 4.10, and each of the points on the line is one window of analysis. Windows from $0 - 1\mu s$, $1\mu s - 2\mu s$ and $2\mu s - 3.5\mu s$. Concrete sample with no damage.

4.2.2.2 DAE - results

Figure 4.13 shows the delay as percentage of the reference transmission time. The lines correspond to one frame of Figures 4.12, A.6 and A.7 respectively. The three points on each line correspond to the early, middle and late window of analysis. Interestingly, the first and second parts of the increasing and decreasing parts of the strain cycle are self-similar. The second part of increasing cycle is almost identical to the first, only with a shift in strain level. This is also the case for the decreasing parts of the strain cycle. Furthermore, the changes in delay are quite large, with an almost 2% difference between the fastest and slowest points on the figure. On the other hand, having delays that are on the scale of a few percent, as opposed to well over 20%, that has been the case for many of the previous figures, is much more realistic. It is worth reiterating that these delays and figures are calculated and created using the exact same method for all concrete samples.

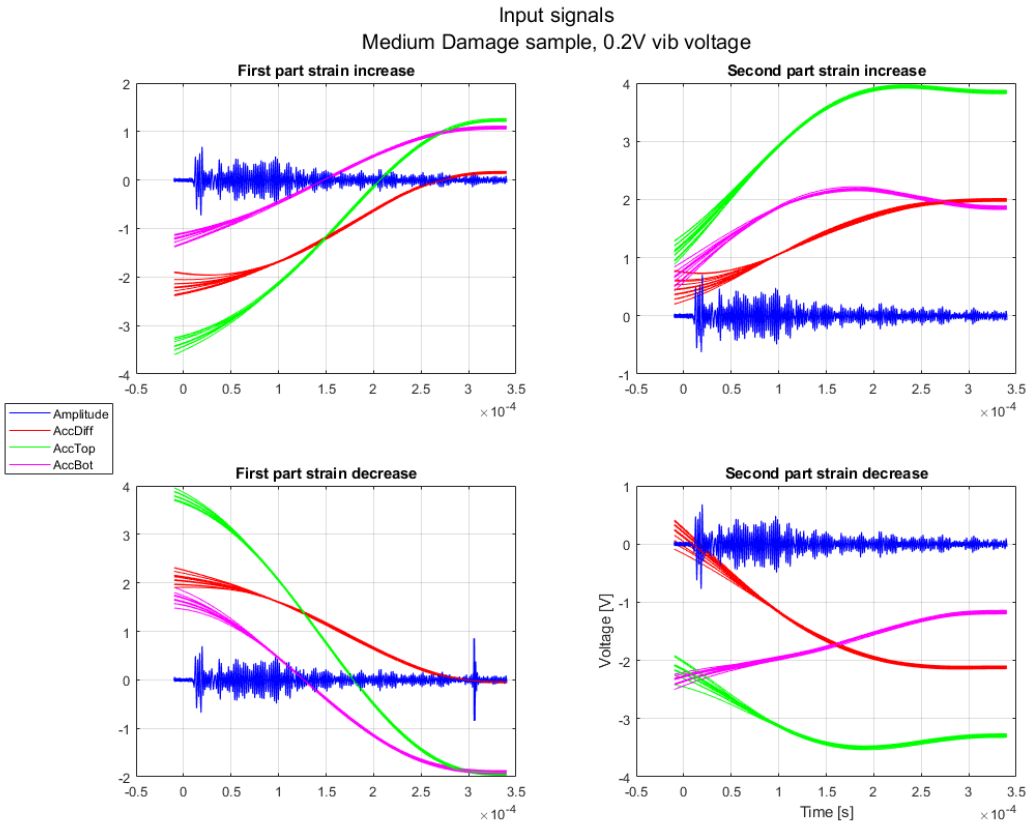

Figure 4.12: All gathered signals from coda measurements of the concrete sample with medium damage, for vibration voltage input of $0.2V$. The plots are divided into the first and second parts of the increasing and decreasing parts of the strain cycle.

4.2.3 Severly damaged

4.2.3.1 Vibration behaviour

Figure 4.14 contains all signals collected for the concrete sample with severe damage, with vibration voltage input of $0.2V$. Similarly to previous figures of the same type, there is a clear flattening of the acceleration curves towards the end of the measurement window. The accelerations measured at the top and bottom of the sample are in phase for this sample, just as it was for the direct sound measurements. As can be observed, there is a much higher acceleration voltage for both the top and bottom accelerometer as compared to the other concrete samples. However, the difference between the top and bottom accelerometer is similar in size as it is for the other concrete samples. The acceleration at the top and base of the sample seems to be fairly in phase.

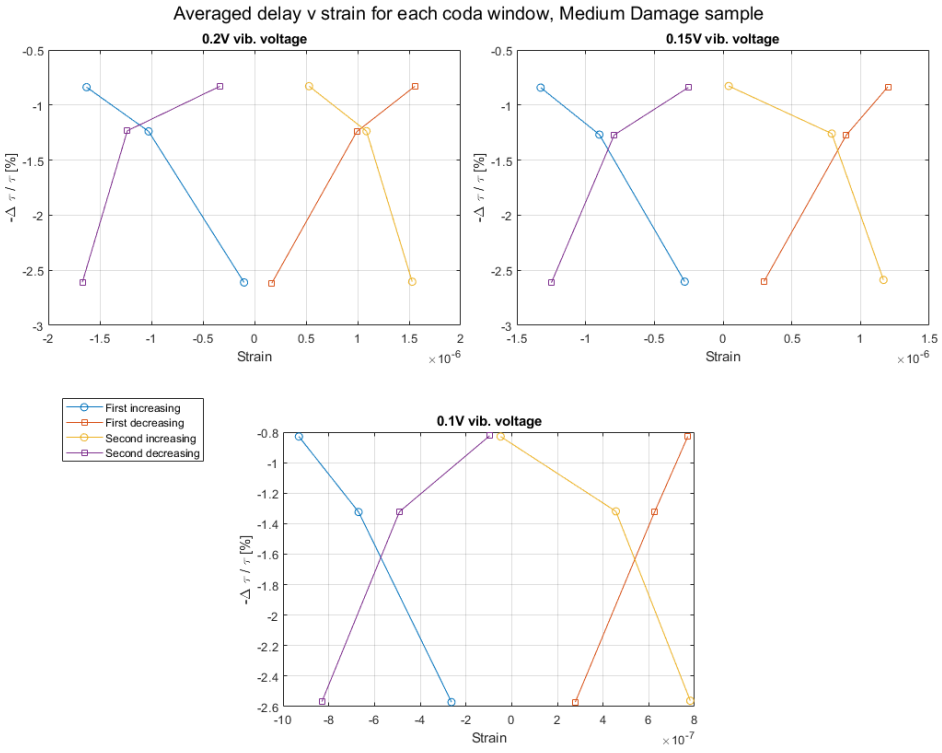

Figure 4.13: Delay as percentage of the reference transmission time plotted as the function of average strain for each of the three vibration voltage inputs. Each line corresponds to one of the the four subplots in Figure 4.10, and each of the points on the line is one window of analysis. Windows from $0 - 1\mu s$, $1\mu s - 2\mu s$ and $2\mu s - 3.5\mu s$. Concrete sample with medium damage.

4.2.3.2 DAE - results

Figure 4.15 contains the delays measured, plotted as percentage of the reference transmission time against the average strain level. Just as for previous figures of the same type, each line corresponds to the first or second measured part of the increasing or decreasing parts of the strain cycle. The values gathered for vibration voltage inputs of $0.15V$ and $0.1V$ are completely unrealistic. For vibration voltage input of $0.2V$, the difference between the fastest and slowest measured delay, about one tenth of one percent of the reference transmission time, seems fairly realistic. However, that this variation of less than one tenth of one percent should be centered around a decrease in sound speed of 64.4% is fairly unrealistic. The ultrasound amplitude was notably smaller than for the other concrete samples. This may have contributed to the unrealistic DAE results. Ignoring the centre around which the delays vary, the behaviour exhibited with vibration voltage input of $0.2V$ is quite similar to the one seen in the sample with medium damage.

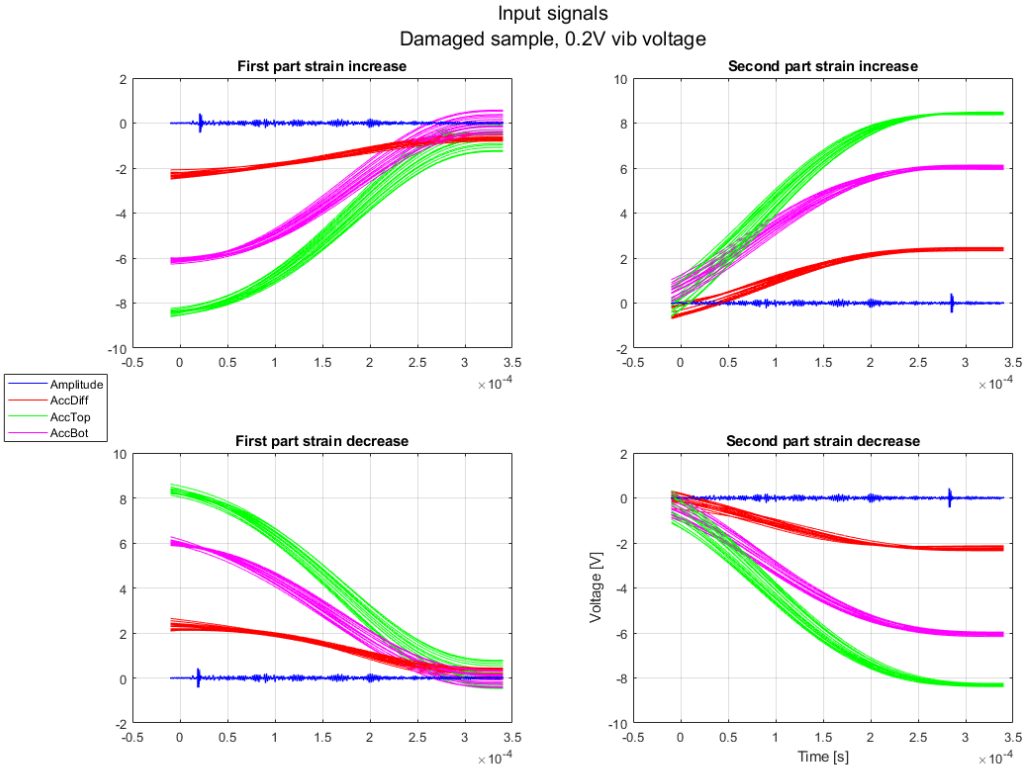

Figure 4.14: All gathered signals from coda measurements of the concrete sample with severe damage, for vibration voltage input of $0.2V$. The plots are divided into the first and second parts of the increasing and decreasing parts of the strain cycle.

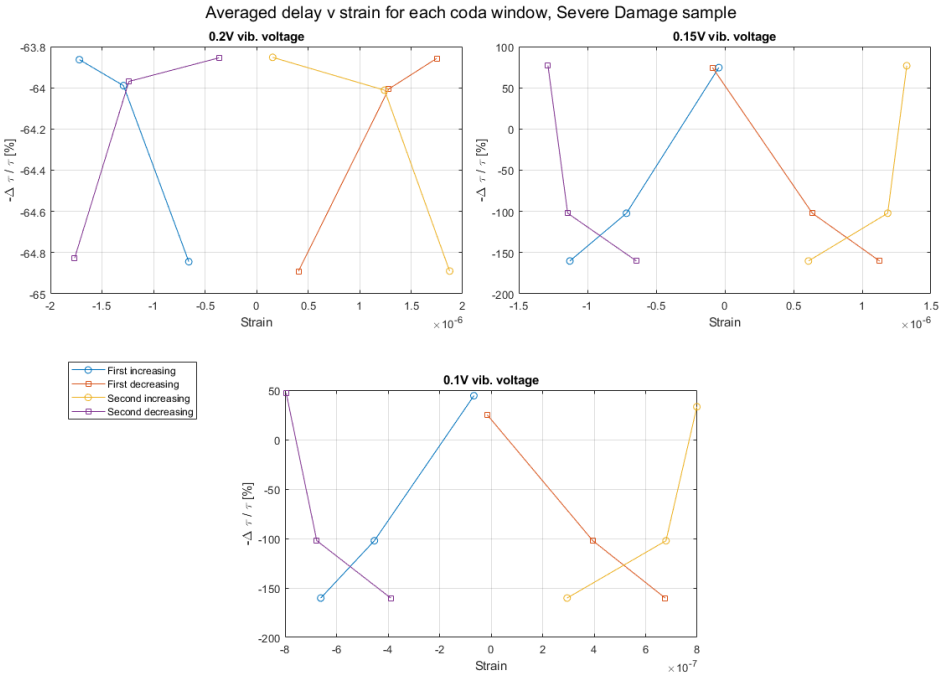

Figure 4.15: Delay as percentage of the reference transmission time plotted as the function of average strain for each of the three vibration voltage inputs. Each line corresponds to one of the the four subplots in Figure 4.10, and each of the points on the line is one window of analysis. Windows from $0 - 1\mu s$, $1\mu s - 2\mu s$ and $2\mu s - 3.5\mu s$. Concrete sample with severe damage.

Chapter 5

Discussion

It is clear that both methods applied at this point show some serious flaws. There is a clear need for further development before either method can be used to study the nonlinearities of concrete under vibration in a rigorous manner. The aim of this master thesis was to *develop* methods of testing. This was unfortunately not possible, as the equipment needed to perform measurements did not become available until 6 days before the original deadline. Thus, two methods of measurement were created, but time did not allow for much further development. Time spent preparing for measurements is much less valuable when developing a measurement method than time with the measurement equipment, and time to analyze and improve measurements in between attempts. All data presented was gathered June 17th. Had there been an opportunity to perform measurements, analyze those measurements, and subsequently improve the method, gather more data and improve the analysis, it is likely that the finished product would have been significantly better. Unfortunately, equipment breaks and it turns out that repairing a piezoelectric vibration element such as the one used for these measurements is a very time consuming matter. The main part of the following discussion will as a result of the circumstances be devoted to the sources of error. The further development section describes some measures through which these sources of error can be addressed, and what could have been the continued effort to further improve these measurement techniques.

5.1 Sources of error

5.1.1 Sampling of phase-degrees in direct sound measurements

The concept behind the algorithm through which the burst period of the direct sound measurements was in the very least a visually pleasing one. As the vibration voltage used was a sine wave, it did not seem infeasible that one could determine a burst period through which one could achieve sampling of an arbitrary amount of phase-points. By

considering the minimum amount of time needed to sample all intended phases and then dividing that time into as many parts as desired phases, the result should be a burst period that perfectly samples all the phases and then repeats, allowing for repetitions that can be averaged for a more precise result. This algorithm failed to translate into practical application due to in particular two factors. Firstly, even though the vibration voltage input may be a perfect sine wave, the resulting acceleration clearly was not. Movement in the base-plate, phase differences, and possible pogo-motion in the compression stack all contributed to a resulting strain field that could not be sampled perfectly in the fashion intended. Secondly, the algorithm used to calculate this supposed perfect burst period had some rounding involved, which may have proved fatal for its use. The signal generator used to generate the burst takes integer value inputs, and there is no guarantee for the perfect burst period to be an integer value of microseconds. The result was, as became abundantly clear from Figures 4.5,4.2 and 4.8, repeated sampling of the strain field that was not as equal in strain as intended.

5.1.2 Stack movement

As Figures 4.4, 4.1 and 4.7 showed, there was significant movement in the base-plate of the stack, as there was a quite large difference between the acceleration atop the sample and the deformation experienced by the sample. One working assumption was that the compressive stack would remain relatively stable under measurements. This was of course not expected to be a completely true assumption, but the degree to which it failed was not expected. For all samples, as can be seen from Figures 4.12, 4.10 and 4.14, the maximum accelerometer difference was $2V$. However, the maximum measured acceleration from the top accelerometer was four times this. The physical consequence of this is that the vibration energy supposed to impose strain on the sample ends up in large part just moving it. It is not clear what action can be taken to remedy this, but a significantly heavier base-plate might be a place to start. A second action that can be taken might be to impose as much confining pressure as the stack will allow. By fear of large resonance responses and considering the maximum capacity of the compressive frame being $50KN$, the confining pressure was kept at around $30KN$.

5.1.3 Low pass-filtering

At the end of each of the coda measurements, there was a clear flattening of the acceleration curves, as can be seen from Figures 4.12, 4.10 and 4.14. At the time of writing, the working theory is that this flattening is the result of the low-pass filtering process. The reasoning behind this conjecture is that this flattening happens regardless of where in the strain cycle the sampled signals are. Figures 4.12 and 4.14 have acceleration differences beginning and ending at either $0V$ or $2V$, which corresponds to the middle or the extremity of the strain cycles. Figure A.4 on the other hand, shows acceleration differences that cross $0V$ without flattening. This suggests that the flattening has something to do with

the end of the window, and no the physical acceleration itself. The second part of both the strain increase and strain decrease cycle shown in Figure A.4 also show the change of acceleration reversing towards the end of the window and flattening. The result of this flattening is that the strain in the last part of each measured frame is incorrect. This effect is likely to be negligible for the direct sound measurements, as the measured window is so short as to be regarded as equal phase regardless.

5.1.4 Delays

The most substantial errors in these measurements are the delays. The magnitude of most of the calculated delays is far too big. What the root of this issue is, is not so clear however. One of the reasons why the cause of this issue is not as easy to identify as the other sources of error is the fact that for a small minority of measurements, the analysis seemed to provide somewhat believable results all together, for most it produced results that were relatively believable, and for some it produced wildly unbelievable results (that somehow still was visually fairly comparable to the other produced results). The first category is inhabited by the delay v strain results produced by the coda analysis method for the concrete sample of medium damage. The change in sound speed under vibration is small, although much larger than that seen in previous work [11]. The change is nevertheless in the area of a few percent, and not tens of percent. The internal variance is however larger than most of the other results, which may be a physical result, but also may be an artifact of the analysis process. The overall lack of reliability of the rest of the results due however contribute to a scepsis regarding the reliability of these results as well.

There are several factors suspected of contributing to the general failure of the delay calculations. Firstly, there was a significant resampling performed for all measurements apart from the coda measurements of the pristine sample. The coda measurements of the concrete sample with no damage were calculated against the average of themselves, as the reference measurement file was corrupted. Thus, there was no need for resampling. For the rest of the measurements, the coda measurements were resampled by a factor of $3750/926$, as the sampling frequency of the reference measurements were $375MHz$, and the sampling frequency of the measurements with vibration was $92.6MHz$. For the direct sound measurements, the sampling frequency was $32.1MHz$, resulting in a resampling of factor $3750/321$. The same reference signal was used for both coda and direct sound measurements, it was however windowed to have the same length as the direct measurement in the second case. The process of resampling may have contributed to the large discrepancies. This was investigated shallowly, and although it may have contributed to the errors, is likely not the sole culprit.

The second contributing factor suspected of influencing the results is the oscilloscope and the triggering mechanism. As can be seen from all included figures featuring a time-axis, all signals begin before $t = 0$. They do however, not all begin with the same exact offset. The reason for this is that when performing the measurements, the trigger signal from the signal generator was late. As seen from the figures SETT INN ASRBHKEWAFJSKBAD,

Table 5.1: Table of first time samples.

Measurement	Direct	Reference	Coda
No damage 0.2 V	-1.4808e-05	-7.0727e-06	-1.4808e-05
No damage 0.15 V	-1.4808e-05	-6.7607e-06	-9.8837e-06
No damage 0.1 V	-1.4808e-05	-7.0727e-06	-9.8837e-06
Medium, 0.2 V	-9.8869e-06	0	-9.8837e-06
Medium 0.15 V	-9.8869e-06	0	-9.8837e-06
Medium 0.1 V	-9.8869-06	0	-9.8837e-06
Severe 0.2 V	-2.1372e-05	0	-9.8837e-06
Severe 0.15 V	-3.8872e-05	0	-9.8837e-06
Severe 0.1 V	-3.8872e-05	0	-9.8837e-06

the input signal was included in the data collection. When setting the starting point of the oscilloscope to $t = 0$, the input signal was not entirely included. This is an issue that surely could be resolved if the available time allowed for several measurement attempts. In order to include the entire input signal, a time offset was set. The first time sample varied between measurements. A table of the all the first time samples are included in Table 5.1. This issue is likely to be major contributing factor to the erroneous delays, but as it was discovered 48 hours before the deadline, and literally whilst writing this paragraph, there was not enough time remaining to correct the issue.

While the varying time offsets likely accounts for much of the constant error in the delays it does not account for the errors in Figures 4.15, for vibration voltage inputs of $0.15V$ and $0.1V$. The third likely source of error is the low ultrasonic signal amplitude present in the measurements of the severely damaged sample. This could have been remedied by a simple sensitivity adjustment on the oscilloscope.

5.1.5 Time constraint

The most important source of error in the results provided in this master thesis is the time constraint. As alluded to in the introduction to this chapter, time, or the lack thereof, played a significant part in providing results that were far from being optimized. The aim of this thesis was to contribute to the field of Non-Destructive Testing of concrete by developing measurement techniques through which one could study the nonlinearities in the elastic response reliably. As the measurement equipment was defective or unavailable throughout the semester in which these techniques were to be developed, and measurements were possible to take *six* days before the original deadline, the time constraint is a source of error worth mentioning. The previously mentioned sources of error could have been remedied, if there was time to perform measurements, analyze the results, perform new measurements and improve the methods through an iterative process. This was not possible. As such, I put forth the time constraint on equipment availability as a source of error to this thesis.

5.2 Further development

Although the provided results are in themselves far from being satisfactory, there are indications as to how further measurement technique can be developed. In order to improve the the direct sound measurements, the burst period algorithm needs to be improved. As nonlinearities in the elasticity response is the desired measured result, assuming the vibration will be linear is not an assumption worth keeping. This can be seen both in Figure 4.3, where the deformation response is distorted and phase shifted compared to the input voltage (which is monitored by the top accelerometer), and by the intended equal strain Figures 4.5, 4.2 and 4.8. A more fruitful approach might lie in taking further inspiration from previous work, and choosing a burst period that is incongruous to the vibration period [11]. However, it seems like the most promising approach is to use the full ultrasonic response of the sample, as is done when measuring using the coda analysis technique. In this thesis, three windows are applied. However, instead of using three separate time windows, a gliding correlation function could be applied to produce phase-resolution greater than that provided by the direct sound measurements. As the ultrasonic signal coda observes changes in the elasticity for as long as it is is contained in the sample, it is likely a significant amount of information to be extracted from the signal coda. There is much work to be done in order to definitively determine how this signal coda should be categorized in terms of strain level. For instance, the latest part of the signal coda included in the measurements performed during this thesis work experiences a quarter period of varying strain. What strain level the last part of signal distinguishable from noise should be classified as having is by no means clear to the author. However, averaging the strain level over the window applied to analyze seemed, especially in the case of $0.1V$ vibration voltage input, as shown in Figure 4.11, to provide a results that at least in relative behaviour complied with the hysteresis model of elasticity. Furthermore, the need for separate reference measurements is, at least, suggested by the results provided for the concrete sample with no damage. As the measurements for this sample were compared to a reference which was the average of all the measurements taken, and provided promising results, suggests that as long as the deformation remains in the elastic regime, there is no need for a separate reference measurement. By considering a far extension of this work, should there be such far developments to these techniques, such that it may be applied to for instance bridges, the strain levels present during such field measurements would be far within the elastic regime. As such, using an average strain level measurement as reference may provide a robust method of studying the elastic response, in particular when the vibrational input is more complicated than a pure sine wave.

Chapter 6

Conclusion

Measurements of the varying ultrasonic sound speed in concrete as a function of imposed strain were performed June 17th 2021. The concrete samples were placed in a compressive frame with a confining pressure of $28KN$ and subjected to an additional varying strain, resulting in a maximum additional strain of $\pm 1.5\mu\sigma$. The aim was to differentiate the response between concrete samples of different degradation grades, and to compare the efficacy of two different measurement techniques to highlight these differences. One method utilized the direct ultrasonic signal, observing a strain field considered constant throughout the transmission. The second method utilized a time window 10 times larger, analyzing the signal coda. The results were in and of themselves unreliable, in large part to due a signal alignment error in the analysis discovered too close to the deadline to correct for. However, the research performed suggests that further development efforts should focus on honing the coda analysis technique.

Bibliography

[1] New York, C. Scribner's sons (1885), Schliemann, Heinrich, Adler, Felix, Dorpfeld, Wilhelm, Tiryns. The prehistoric palace of the kings of Tiryns, the results of the latest excavations;, Available from https://archive.org/details/bub_gb_pw4BAAAAMAAJ

[2] NRK.no June 2021, Johansen Espeland, Anett, Konserthus-fasade slår sprekker ni år etter åpning Available from https://www.nrk.no/rogaland/stavanger-konserthus-ma-skifte-ut-rod-glassbetong-pa-fasaden-1.15527629

[3] 2021, American Society of Civil Engineers, Infrastructure report card 2021, https://infrastructurereportcard.org/wp-content/uploads/2020/12/Bridges-2021.pdf

[4] Verdens Gang November 2017, De forsømte broene Available from https://www.vg.no/spesial/2017/de-forsomte-broene/inspeksjoner/

[5] Department of Civil Engineering, Fahad Bin Sultan University, Tabouk Saudi Arabia, Tantawi, Hasan. (2015). Introduction to Concrete Technology. 10.13140/RG.2.1.3219.9201. Available from: https://www.researchgate.net/publication/275464135_Introduction_to_Concrete_Technology

[6] Hydrotechnical Construction 4, 448–453 (1970). Tsiskreli, G.D., Dzhavakhidze, A.N. The effect of aggregate size on strength and deformation of concrete. Available from: https://doi.org/10.1007/BF02376145

[7] Theses and Dissertations. 3000. LeBow, Caleb Joshua, "Effect of Cement Content on Concrete Performance" (2018). Available from: https://scholarworks.uark.edu/etd/3000

[8] Advances in Materials Science and Engineering. 2014. 1-11. 10.1155/2014/273460, Kim, Yun-Yong Lee, Kwang-Myong Bang, Jin-Wook Kwon, Seung-Jun. (2014). Effect of W/C Ratio on Durability and Porosity in Cement Mortar with Constant Cement Amount. Available from: https://www.researchgate.net/publication/275071553_Effect_of_WC_Ratio_on_Durability_and_Porosity_in_Cement_Mortar_with_Constant_Cement_Amount

[9] Doctoral Thesis at NTNU, 2013:375, Nonlinear Elastic Waves for Estimation of Rock Properties, Stroisz, Anna Magdalena, Trondheim, December 2013

[10] Boston University, Mechanical Engineering, Mechanics of Materials: Strain, https://www.bu.edu/moss/mechanics-of-materials-strain/

[11] Journal of Applied Physics. 114., Rivière, Jacques Renaud, Guillaume Guyer, Robert Johnson, P.. (2013). Pump and probe waves in dynamic acousto-elasticity: Comprehensive description and comparison with nonlinear elastic theories. 10.1063/1.4816395. Available from: https://www.researchgate.net/publication/257975856_Pump_and_probe_waves_in_dynamic_acousto-elasticity_Comprehensive_description_and_comparison_with_nonlinear_elastic_theories

Appendix A

Additional figures

A.1 All sampled points of direct sound DAE measurements

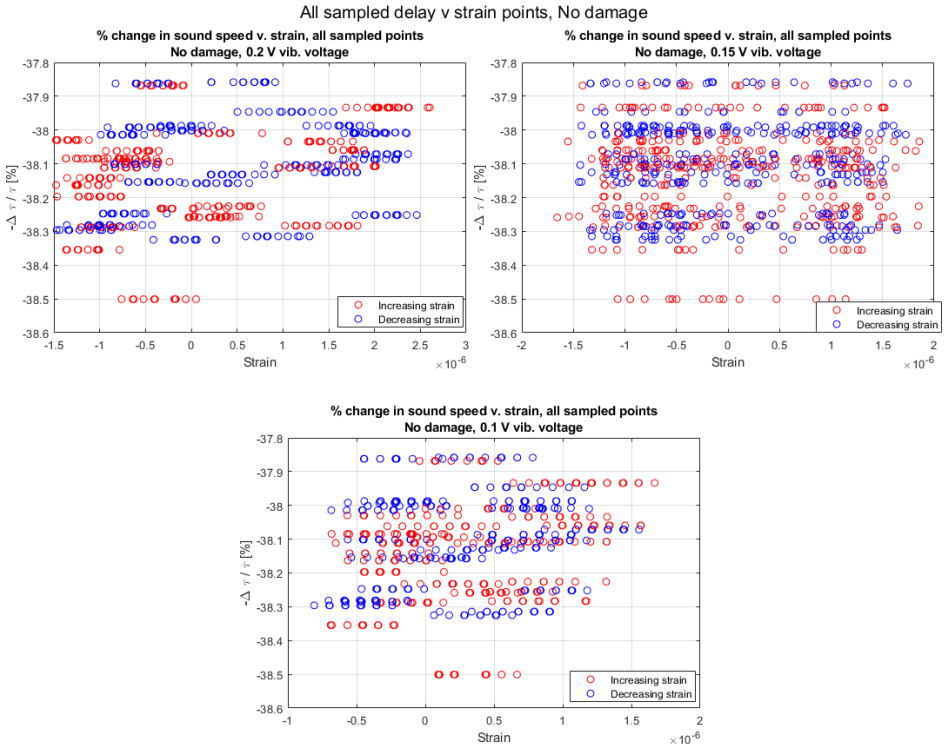

Figure A.1: All sampled delays in percent relative to the reference transmission time plotted against the average strain of the time window the delays are sampled from. Concrete sample with no damage.

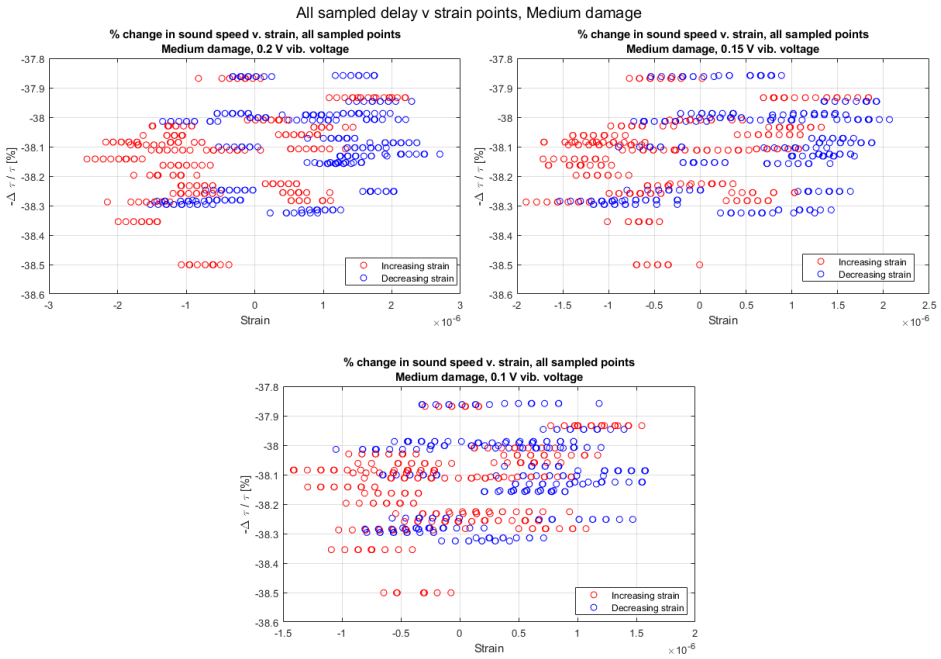

Figure A.2: All sampled delays in percent relative to the reference transmission time plotted against the average strain of the time window the delays are sampled from. Concrete sample with medium damage.

A.2 Coda-measurement data

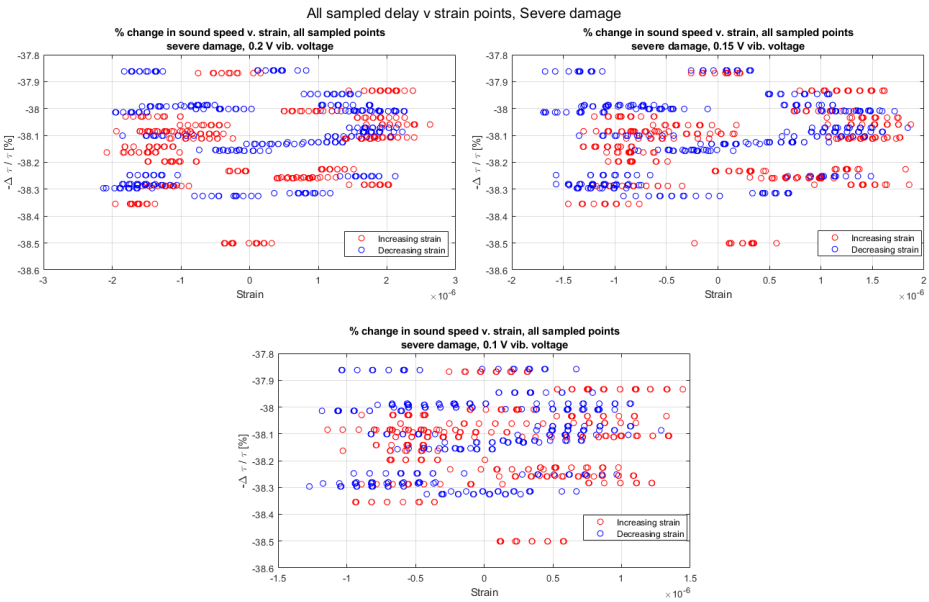

Figure A.3: All sampled delays in percent relative to the reference transmission time plotted against the average strain of the time window the delays are sampled from. Concrete sample with severe damage.

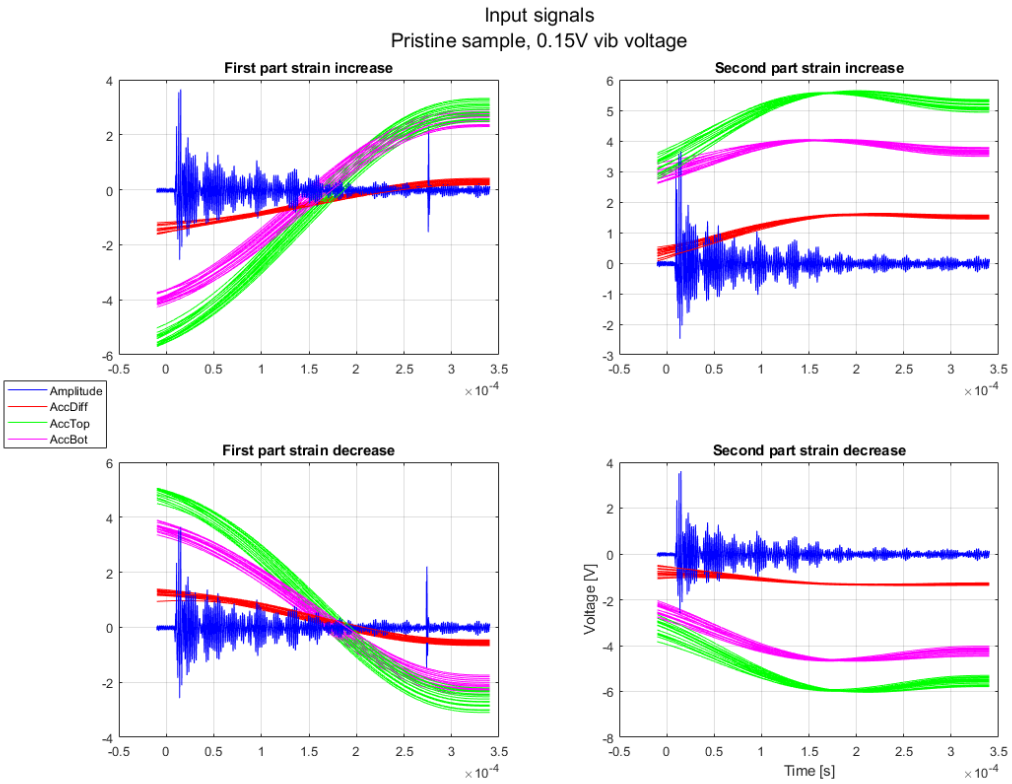

Figure A.4: All gathered signals from coda measurements of the concrete sample with no damage, for vibration voltage input of $0.15V$. The plots are divided into the first and second parts of the increasing and decreasing parts of the strain cycle.

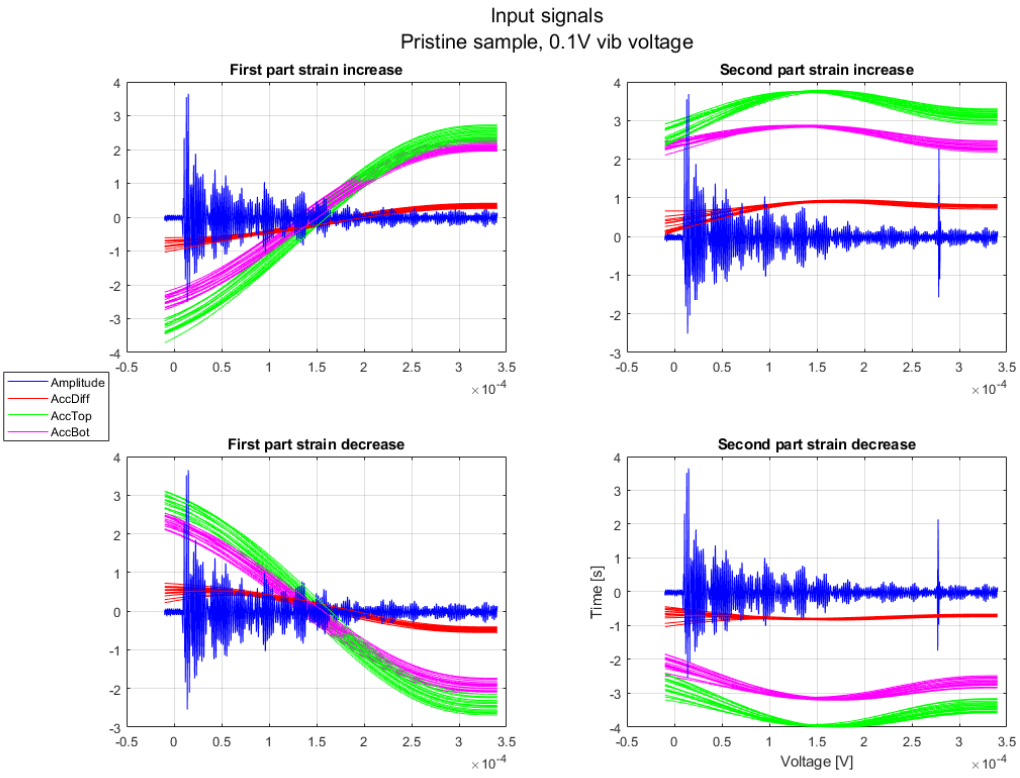

Figure A.5: All gathered signals from coda measurements of the concrete sample with no damage, for vibration voltage input of $0.11V$. The plots are divided into the first and second parts of the increasing and decreasing parts of the strain cycle.

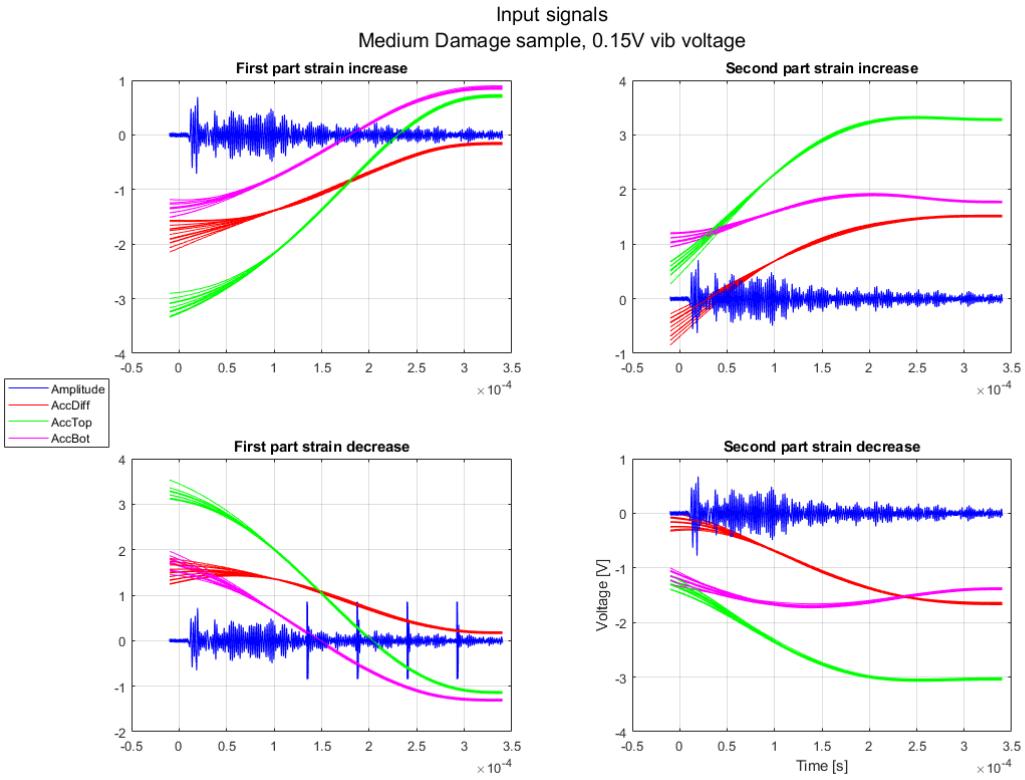

Figure A.6: All gathered signals from coda measurements of the concrete sample with medium damage, for vibration voltage input of $0.15V$. The plots are divided into the first and second parts of the increasing and decreasing parts of the strain cycle.

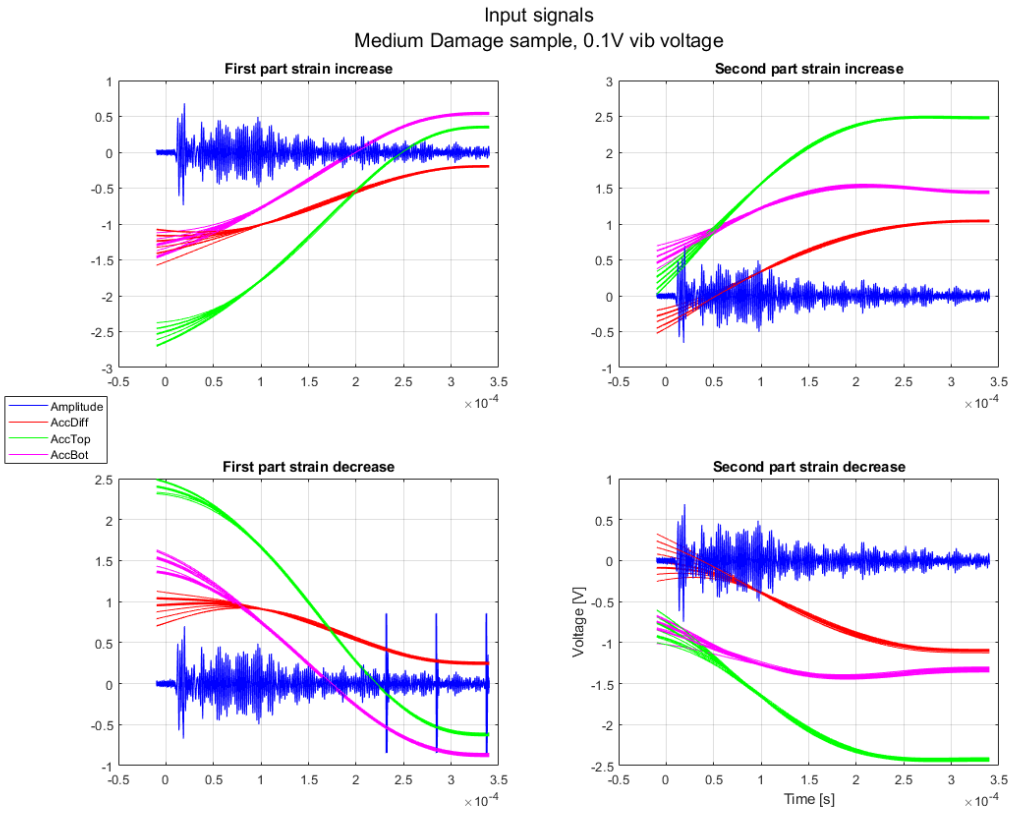

Figure A.7: All gathered signals from coda measurements of the concrete sample with mediun damage, for vibration voltage input of $0.1V$. The plots are divided into the first and second parts of the increasing and decreasing parts of the strain cycle.

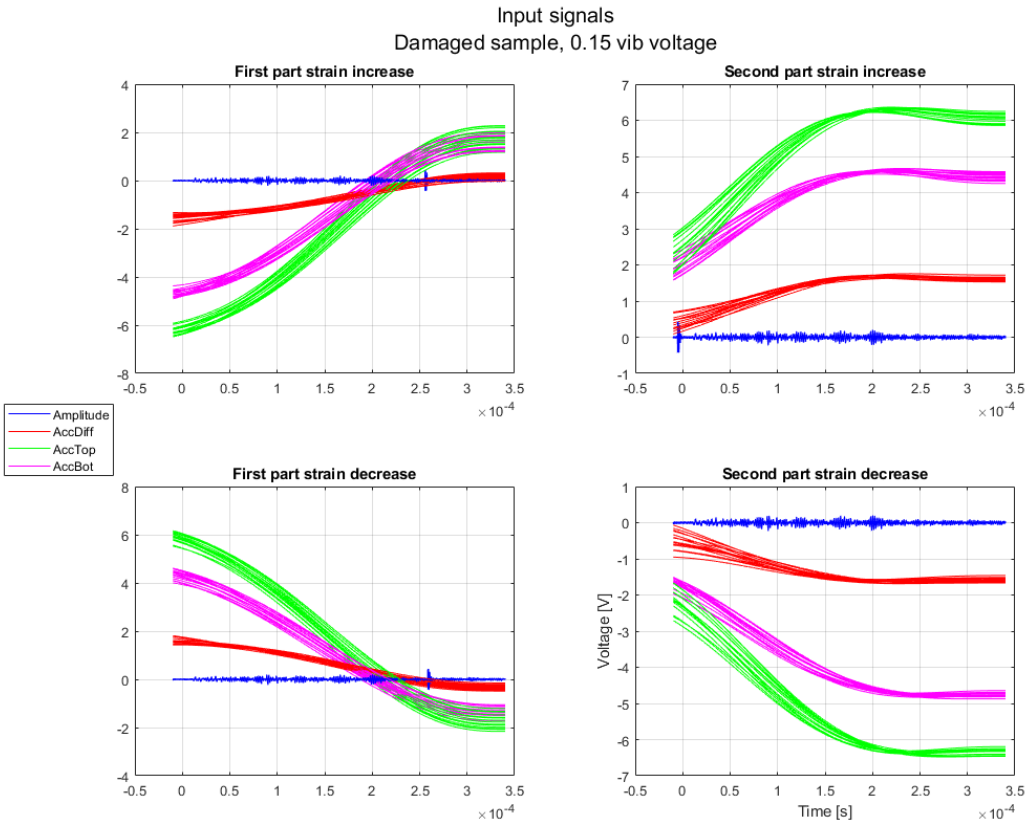

Figure A.8: All gathered signals from coda measurements of the concrete sample with severe damage, for vibration voltage input of $0.15V$. The plots are divided into the first and second parts of the increasing and decreasing parts of the strain cycle.

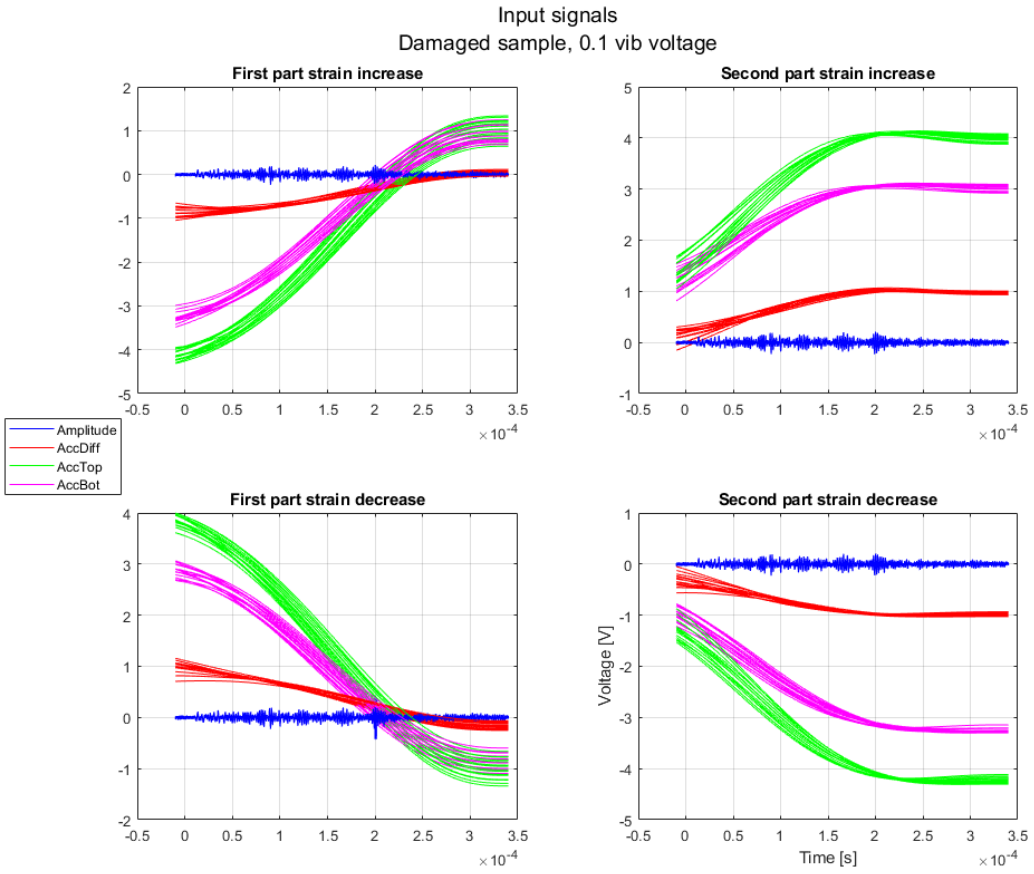

Figure A.9: All gathered signals from coda measurements of the concrete sample with severe damage, for vibration voltage input of $0.1V$. The plots are divided into the first and second parts of the increasing and decreasing parts of the strain cycle.

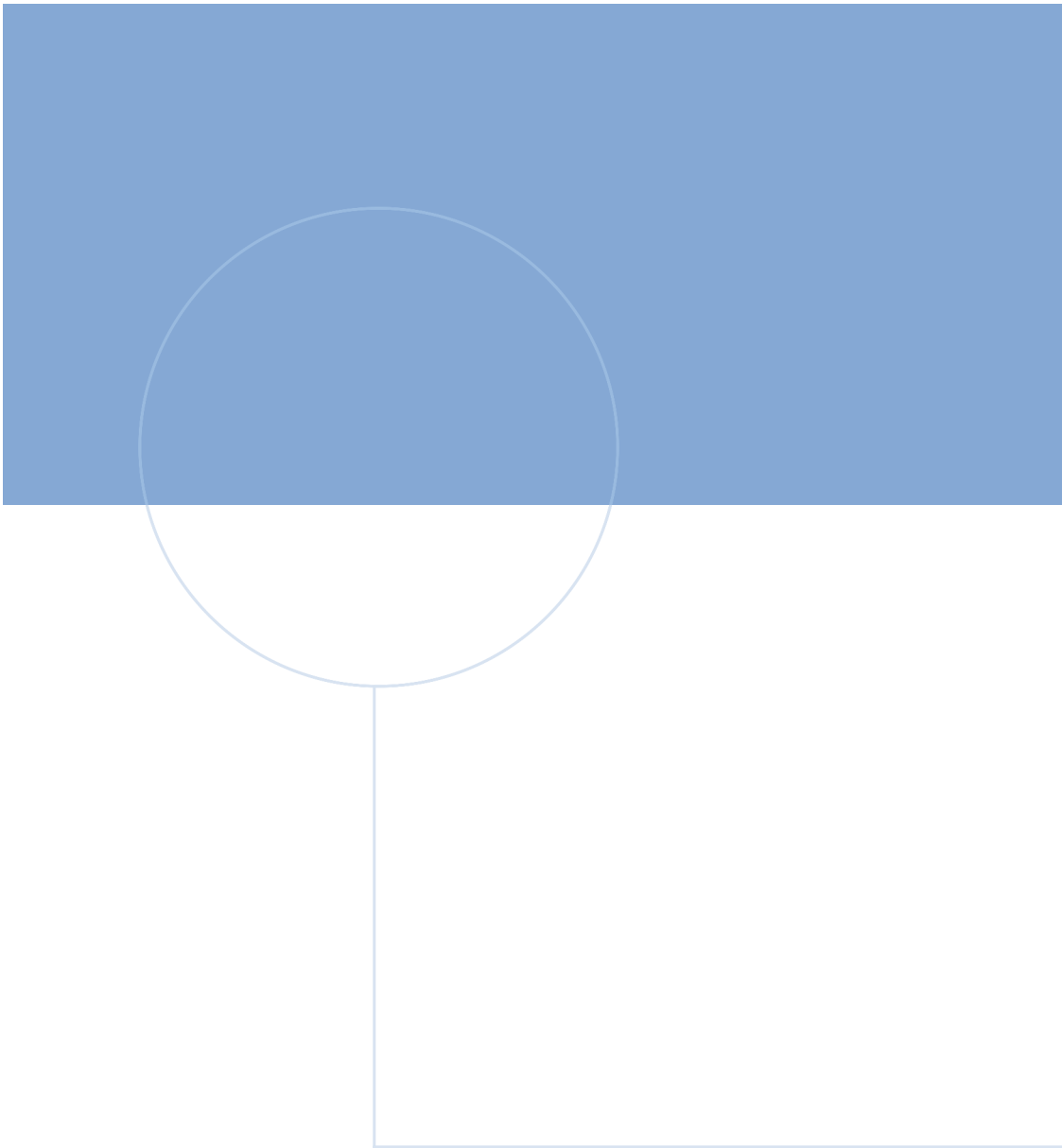

NTNU

Norwegian University of
Science and Technology